UNIVERSITY OF LEEDS

This is a repository copy of *Exhumed lateral margins and increasing flow confinement of a submarine landslide complex*.

White Rose Research Online URL for this paper:
http://eprints.whiterose.ac.uk/121509/

Version: Accepted Version

Article:

Brooks, HL, Hodgson, DM orcid.org/0000-0003-3711-635X, Brunt, RL et al. (2 more authors) (2018) Exhumed lateral margins and increasing flow confinement of a submarine landslide complex. Sedimentology, 65 (4). pp. 1067-1096. ISSN 0037-0746

https://doi.org/10.1111/sed.12415

© 2017 The Authors. Sedimentology © 2017 International Association of Sedimentologists. This is the peer reviewed version of the following article: Brooks, H. L., Hodgson, D. M., Brunt, R. L., Peakall, J. , Flint, S. S. and Trofimovs, J. (2018), Exhumed lateral margins and increasing flow confinement of a submarine landslide complex. Sedimentology, 65: 1067-1096. doi:10.1111/sed.12415, which has been published in final form at https://doi.org/10.1111/sed.12415. This article may be used for non-commercial purposes in accordance with Wiley Terms and Conditions for Self-Archiving. Uploaded in accordance with the publisher's self-archiving policy.

Reuse

Items deposited in White Rose Research Online are protected by copyright, with all rights reserved unless indicated otherwise. They may be downloaded and/or printed for private study, or other acts as permitted by national copyright laws. The publisher or other rights holders may allow further reproduction and re-use of the full text version. This is indicated by the licence information on the White Rose Research Online record for the item.

Takedown

If you consider content in White Rose Research Online to be in breach of UK law, please notify us by emailing eprints@whiterose.ac.uk including the URL of the record and the reason for the withdrawal request.

White Rose university consortium
Universities of Leeds, Sheffield & York

eprints@whiterose.ac.uk
https://eprints.whiterose.ac.uk/

ACCEPTED MANUSCRIPT- SEDIMENTOLOGY

Exhumed lateral margins and increasing infill confinement of a submarine landslide complex

Hannah L. Brooks [1]*, David M. Hodgson [1], Rufus L. Brunt [2], Jeff Peakall [1], Stephen S. Flint [2]

[1] Stratigraphy Group, School of Earth and Environment, University of Leeds, Leeds, UK, LS2 9JT

[2] Stratigraphy Group, School of Earth and Environmental Sciences, University of Manchester, Manchester, M13 9PL, UK.

Corresponding author: eehlb@leeds.ac.uk

Key words: submarine landslide; slope failure; basal shear surface; basal shear zone; lateral margin

ABSTRACT

Submarine landslides, including the basal shear surfaces along which they fail, and subsequent infill, are commonly observed in modern seafloor and seismic reflection datasets. Their resultant relief impacts sediment routeing and storage patterns on continental margins. Here, three stacked submarine landslides are documented from the Permian Ecca Group, Laingsburg depocentre, Karoo Basin, South Africa, including two superimposed lateral margins. The stratigraphic framework includes measured sections and correlated surfaces along a 3 km long, 150 m high outcrop. Two stacked 2.0-4.5 km wide and 90 m and 60 m deep erosion surfaces are recognised, with lateral gradients of 8° and 4° respectively. The aim of this study is to understand the evolution of a submarine landslide complex, including: evolution of basal shear surfaces/zones; variation of infill confinement; and location of the submarine landslides in the context of basin-scale sedimentation and degradation rates.

Three stages of formation are identified: 1) failure of submarine landslide 1, with deposition of unconfined remobilized deposits; 2) failure of submarine landslide 2, forming basal shear surface/ zone 1, with infill of remobilized deposits and weakly confined turbidites; and 3) failure of submarine landslide 3, forming basal shear surface/zone 2, with infill of remobilized deposits and confined turbidites, transitioning stratigraphically to unconfined deposits. Basal shear varies laterally, from metres thick zones in silt-rich strata to sharp, to discrete stepped surfaces in sand-rich strata. Faulting and rotation of overlying bedding suggest that the shear surfaces/zones were dynamic.

Stacking of landslides resulted from multiphase slope failure, increasing down-dip topography, and confinement of infilling deposits. The failure slope was likely a low supply tilted basin margin evidenced by megaclast entrainment from underlying basin-floor successions and the lack of channel systems. We develop a generic model of landslide infill, as a function of sedimentation and degradation rates, which can be applied globally.

INTRODUCTION

Submarine landslides degrade and reshape continental margins, and can cover areas of thousands of square kilometres (e.g. McAdoo *et al.,* 2000; Frey-Martinez *et al.,* 2005; Moscardelli *et al.,* 2006; Moscardelli & Wood, 2008, 2015). Their catastrophic nature means they can destroy seabed infrastructure (Locat & Lee, 2002; Hoffman *et al.,* 2004; Shipp *et al.,* 2004; Masson *et al.,* 2006) and have the potential to disrupt the overlying water column to form tsunamigenic waves (e.g. Pelinovsky & Poplavsky, 1996; Driscoll *et al.,* 2000; Løvholt *et al.,* 2005). The quasi-instantaneous modification of the seascape by these events leads to the rerouteing, capture and ponding of subsequent flows (e.g. Alves & Cartwright, 2010; Ortiz-Karpf *et al.,* 2015; Kneller *et al.,* 2016; Fallgatter *et al*., 2017; Qin *et al.,* 2017). Therefore, understanding the formation and infill of major submarine landslides is required to assess their geohazard potential, and the stratigraphic evolution of continental margins. Submarine landslides on the modern seabed, and buried examples imaged in reflection seismic data, illustrate their wide range of scales, geometries, run out distances, and return periods (e.g. Bellaiche *et al*., 1986; Normark & Gutmacher, 1988; Normark, 1990; Gee *et al.,* 2001; Masson *et al.,* 2002; Hürlmann *et al.,* 2004; Haflidason *et al.,* 2004; Solheim *et al.,* 2005; Frey-Martinez *et al.,* 2006; Jackson, 2011; Baeten *et al.,* 2013; Hunt *et al.,* 2013; Laberg *et al.,* 2014; Alfaro & Holz, 2014; León *et al.,* 2017).

Submarine landslides move down-slope across a basal shear surface (*sensu* Bull *et al.,* 2009), also referred to in previous studies as a glide-, failure-, slip- or basal shear plane (e.g. Alves, 2010; Masson *et al.,* 2010; Baeten *et al.,* 2014), or a detachment or décollement surface (e.g. Vanneste *et al.,* 2006). The basal shear surface develops due to progressive shear failure (Varnes, 1978; Bull *et al.,* 2009), and extensive substrate entrainment leads to downslope increases in flow volume (bulking) (Prior *et al*., 1984; Gee *et al.*, 2006; Dykstra *et al.*, 2011; Joanne *et al.,* 2013; Ortiz-Karpf *et al.,* 2017a). Lateral margins are part of the basal shear surface, and typically form steep planar surfaces (e.g. Fig. 1) perpendicular or sub-parallel to the direction of net displacement (Frey-Martinez *et al*., 2006; Bull *et al.,* 2009; Gamberi *et al*., 2011; Alves, 2015; Ortiz-Karpf *et al*., 2017a). Basal shear surfaces can have a thickness forming a basal shear zone (*sensu* Alves & Lourenço, 2010), and can be modified by further failure events, creating complex and composite features, which can be later modified by differential compaction (Alves, 2010). Failed material from the landslide found above and beyond the basal shear surface (Hampton *et al.,* 1996; Frey-Martinez *et al.,* 2005) consists of slides, slumps and debris flows (Varnes, 1958) and their spatial transitions (Martinsen, 1994) with deposits collectively referred to as remobilized deposits. These individual failure events are equivalent to mass transport deposits (MTDs) in studies focused on reflection seismic datasets, which stack to form mass transport complexes (MTCs). Failures can form a single submarine landslide or a composite landslide complex (e.g. Gee *et al*., 2006; Antobreh & Krastel, 2007; Li *et al.,* 2017) with products of failure often treated as multiple separate events (MTDs) in seismic and outcrop datasets (e.g. Moscardelli *et al.,* 2006; Sobiesiak *et al.,* 2016; Ortiz-Karpf *et al*., 2017b).

Understanding of the evolution of submarine landslides and their impact on subsequent flow processes is limited by the low vertical resolution and lithological calibration from modern and subsurface examples. Detailed information on the substrate lithology, the basal shear surface or zone, and the sedimentology and stratigraphic architecture of overlying strata can be provided by exhumed examples (e.g. Martinsen, 1989; Martinsen & Bakken, 1990; Lucente & Pini, 2003; Pickering & Corregidor, 2005; Spörli & Rowland, 2007; Callot *et al.,* 2008; King *et al.,* 2011). These examples permit the character and evolution of the basal shear surface or zone (e.g. Alves & Lourenço, 2010; Dakin *et al*., 2013), and process interactions between subsequent flows and submarine landslide relief (e.g. Armitage *et al.,* 2009; Jackson & Johnson, 2009; Ortiz-Karpf *et al.,* 2015; Kneller *et al.,* 2016; Sobiesiak *et al.,* 2016; Fallgatter *et al*., 2017), to be investigated. However, exhumed submarine landslide systems of scales comparable to modern and subsurface examples are beyond the scale of most outcrops. For example, large-scale (10s m deep) basal erosion has rarely been demonstrated (e.g. Lucente & Pini, 2003; Shultz *et al.,* 2005; van der Merwe *et al.,* 2009; Dakin *et al*., 2013) and both exhumed lateral margins of basal shear surfaces or zones, and the evolution of flow confinement over multiple submarine landslides, have not been investigated.

This study aims to document a unique example of exhumed deposits of three successive submarine landslides, including the lateral margins of two distinct basal shear surfaces or zones, using a large outcrop of Permian, lower Ecca Group stratigraphy at the distal end of the Laingsburg deep-water system, Karoo Basin, South Africa. Specific objectives are: i) to investigate the evolution of three submarine landslides from basal shear surface or zone erosion and deformation to infill and overspill; ii) to categorise the variations in confinement of remobilized and turbidite components that overlie the basal shear surface or zone; iii) to investigate variations in the basal shear surface or zone across strike; and iv) to consider the context of this example in terms of basin-scale sedimentation and degradation.

GEOLOGICAL BACKGROUND

Karoo Basin and stratigraphy

The Karoo Basin, South Africa (Fig. 2A), has been interpreted as a retroarc foreland basin (Visser & Prackelt, 1996; Visser, 1997; Catuneanu *et al.,* 1998), and more recently as a thermal sag basin that subsequently evolved into a retroarc foreland basin in the Triassic (Tankard *et al.,* 2009). The 8 km thick Karoo Supergroup (Fig. 2C) is subdivided into the Dwyka, Ecca and Beaufort Groups. The Dwyka Group comprises glacial deposits (Late Carboniferous to Early Permian); the Ecca Group clastic marine deposits (Permian); and the Beaufort fluvial deposits (Permian to Triassic).

Basal deposits of the Lower Ecca Group (Fig. 2A) comprise mudstones, chert and shallow marine carbonates of the Prince Albert Formation, overlain by black carbonaceous mudstones of the Whitehill Formation and fine-grained turbidites, cherts and ashes of the Collingham Formation. These formations together average 250 m in thickness and are mapped for 800 km along the southern margin of the Karoo Basin (Viljoen, 1992, 1994; Visser, 1992; Johnson *et al.,* 1997). In the Laingsburg depocentre, the Collingham Formation is overlain by the Vischkuil Formation, which forms the basal section of the 1800 m thick progradational succession through basin-floor deposits (Vischkuil and Laingsburg formations; Sixsmith *et al.,* 2004; van der Merwe *et al.,* 2010), channelized submarine slope (Fort Brown Fm.; Hodgson *et al.,* 2011; Di Celma *et al.,* 2011; Flint *et al*., 2011) to shelf-edge and shelf deltas (Waterford Fm.; Jones *et al.,* 2015; Poyatos-Moré *et al.,* 2016). Regional palaeoflow is towards the NE and E throughout the succession with the entry point to the SW (van der Merwe *et al.,* 2014). The mapping of successive slope-to-basin-floor systems in the Laingsburg depocentre indicates the presence of a lateral, broadly E-W orientated basin margin to the south of the Laingsburg area (van der Merwe *et al.,* 2014). In the east of the Laingsburg depocentre, the Vischkuil and Laingsburg formations thin and pinch out, along with the sand-rich component of the Fort Brown Formation. Around the town of Prince Albert (Fig. 1) the distal reaches of the Vischkuil and Laingsburg formations intercalate with the Ripon Formation, a deep-water system derived from the east (Kingsley, 1981; Visser, 1993). The Ripon Formation deposits are distinctive at outcrop due to their coarser (medium sandstone) grain size.

DATA AND METHODS

Study location

This study focuses on a large outcrop at the distal end of the Laingsburg depocentre (Fig. 2A), located 95 km east of Laingsburg town and 14 km west of Prince Albert (Fig. 2A). The NW-SE orientated outcrop is 3 km in length and 150 m in height. The base of the outcrop is marked by in place strata of the Prince Albert, Collingham and Whitehill formations, which can be traced laterally across an area of 1.5-2 kilometres of either no exposure or intensely tectonically deformed strata, to more continuous outcrops to the east and west of the section (Fig. 2B). Uniquely at this location, both the Collingham and Whitehill formations are cut out over a >1.5 km long section, with highly contorted overlying deposits (Fig. 2B). The overall tectonic shortening direction in the southern Karoo Basin is to the north, with west-east trending and north verging thrust faults and folds that are closely associated with quartz on slip planes. In the study area, the amount of shortening is ~38% (Spikings *et al*., 2015). The structural dip varies from 10° to 40° and the dip direction from NW to NE, and shows minor displacement in the form of a thrust fault in the northeast of the section. Syn-sedimentary deformation is readily identifiable as being bound by undeformed units, and the faults and folds not following the regional tectonic trends outlined above.

Methodology

Twenty long measured sections (up to 150 m), and numerous shorter sections, totalling 1500 m, were logged at cm-scale to document lithology, grain size, sedimentary structures and key stratal boundaries (Figs 2B and 3). The correlation framework is constrained by walking stratigraphic surfaces between sections (Fig. 3) augmented with photopanels compiled using Unmanned Aerial Vehicle photography (Fig. 3B). A laterally continuous sandstone package, a distinctive 10 m thick package of sharp topped, thin-bedded sandstone and siltstone turbidites, which can be traced laterally across 2.5 km of the outcrop, is used as an upper correlation datum (Fig. 3). In addition, a distinctive and uniform bed present throughout the basin-fill known as the Matjiesfontein chert, a laterally extensive 40-50 cm thick white chert bed in the Collingham Formation identified across the SW Karoo Basin (Fig. 3) was used as a basal datum. Palaeocurrent data were collected from ripple cross laminations, flutes and grooves, with fold hinges and bedding plane measurements providing kinematic data within contorted units. Regional-scale measured sections were collected several kilometres either side of the outcrop to constrain the large-scale architecture with general facies associations shown in Figure 2B.

FACIES ASSOCIATIONS

Six facies associations have been classified based on sedimentary facies and interpreted processes.

FA 1: Iron-rich mudstone

This facies association comprises dark-grey, carbonaceous, iron-rich mudstone with common chert nodules, carbonate concretions and large petrified wood clasts. Remobilized mudstone beds are also present within a dark mudstone matrix, usually well cemented and iron rich (Fig. 4A), <50 cm in thickness, folded and/or disaggregated. Packages are >30 m thick with a sharp upper contact with organic-rich mudstone.

Interpretation

FA 1 is the Prince Albert Formation, which was deposited either in a marine basin as shelf deposits (Strydom, 1950; Buhmann *et al.,* 1989; Visser, 1991, 1994), or in a freshwater lake environment (Herbert & Compton, 2007). Prince Albert Formation sediments accumulated from syn- to post-glacial suspension fall-out and flocculation of fines from large inflows of sediment-laden water (Domack, 1983; Smith & Ashley, 1985), with some input by turbidity currents and mud flows of semi-consolidated sediments (Tankard *et al.,* 1982; Visser, 1991).

FA 2: Organic-rich mudstone

This facies association comprises a uniform, laterally continuous, 30 m thick package of organic-rich, black coloured, thinly laminated mudstone (Fig. 4B), which weathers white. The unit has a sharp upper and lower contact with bounding lithostratigraphic units.

Interpretation

FA 2 is the Whitehill Formation, a carbonaceous mudstone (Visser 1979; Tankard, 2009), which formed in anoxic conditions across the Karoo Basin (Oelofsen, 1987), indicating little seabed topography at the time of deposition. The sedimentation rate for the Whitehill Formation is thought to be very low with almost no coarse clastic input in relatively shallow water (Flint *et al.,* 2011).

FA 3: Thinly bedded fine grained turbidites, ash and chert

Interbedded siltstone (<1-30 cm), organic rich/iron cemented beds (Fig. 4C), chert (<40 cm), iron-rich splinter weathered mudstone, sandstone beds (<20 cm) and sandy ash deposits (<1-40 cm) (Fig. 4E). Beds are planar and laterally continuous (Fig. 4F), including the distinctive 45 cm thick Matjiesfontein chert bed, traceable across the outcrop belt (Fig. 4D). Sandstone and coarse siltstone beds with normally graded bed tops contain planar, ripple and climbing ripple lamination. These deposits gradually transition upward into sandstone beds. Packages are up to 30-35 m thick.

Interpretation

The Collingham Formation comprises suspension and turbidity current deposits (Johnson *et al.,* 2006) in a brackish-marine setting (Scheffler *et al.,* 2006; Tankard *et al.,* 2009). Interlayered ashfall tuffs may have derived from volcanoes located in what is now northern Patagonia, where Permian silicic-andesitic volcanic and plutonic rocks crop out (McKay *et al.,* 2015).

FA 4: Sandstone and siltstone turbidites

Interbedded, sharp based and topped siltstone and sandstone beds varying in thickness (<0.01-3 m) with grading ranging from, no grading (Figs 4G and 4I), through weak normal grading, to well graded with siltstone caps (Fig. 4H). Beds are structureless (Fig. 4G) or contain a variety of sedimentary structures including planar (Fig. 4J), ripple and climbing ripple lamination (Figs 4J and 4K), flutes and grooves on bed bases, and a range of dewatering structures including pipes, ball-and-pillow and flame structures. Beds range from laterally continuous to discontinuous with thickening and thinning to pinchout over 10s of metres. Commonly, the more discontinuous beds onlap underlying packages and have widely dispersed palaeocurrent directions. Packages range from 5-50 m thick. Locally, this facies association forms tightly folded and contorted units (transitioning to FA 6) with highly variable fold axis orientations.

Interpretation

Structureless and normally graded sandstones are interpreted as sand-rich high-density turbidity current deposits (Bouma, 1962; Lowe, 1982; Mutti, 1992; Kneller & Branney, 1995). The absence of sedimentary structures indicates rapid deposition and limited development of depositional bedforms. Planar- and ripple-lamination are a product of reworking of the bed beneath low-density turbidity currents (Allen, 1984; Southard, 1991; Best & Bridge, 1992). Dewatering structures are a result of sediment liquefaction (Mulder & Alexander, 2001; Stow & Johansson, 2002). Abrupt thickness changes, onlap and widely dispersed palaeocurrent directions indicate interaction of flows with underlying topography (Kneller *et al*., 1991). Normally graded beds with siltstone caps indicate 3D topographical confinement of turbidites (e.g. Pickering & Hiscott, 1985; Haughton, 1994; Sinclair & Tomasso, 2002; Sinclair & Cowie, 2003). Sharp bed tops and lack of grading suggest deposition in an unconfined setting. Generally, these beds are more laterally consistent in thickness suggesting that depositional processes were not strongly affected by seabed topography. Localised folded and contorted units indicate remobilization.

FA 5: Chaotic deposits

Poorly sorted conglomerate that comprises sub-angular to sub-rounded intrabasinal mudstone clasts (mm – 10s of cm in diameter), mm-scale terrestrial organic material and other remobilized deposits (FA 6; cm's – 100s m in diameter) supported by a matrix of claystone, siltstone and/or sandstone (Fig. 4M). Thicknesses of chaotic packages can vary from 0.5-50 m, and vary laterally and stratigraphically, along with clast size and lithology, forming undulating top surfaces (Fig. 4L).

Interpretation

The poor sorting and matrix-supported fabric indicate cohesive debris flow deposits. Variations in thickness, lithology, and clast size result from changes in lithology of the primary sediment, transport distance and seabed topography. Cohesive freezing of material (Middleton & Hampton, 1976) creates irregular top surfaces.

FA 6: Remobilized deposits

This FA comprises two broad types:

i. Folded strata: Small scale (0.4-5 m) (Figs 4N and 4P) and large scale (up to 80 m amplitude; Fig. 4O) folded sandstone and siltstone beds, exhibiting a variety of shapes, sizes and orientations. Fold attitude varies from upright to recumbent, with interlimb angles from isoclinal to open. Beds are sheared and faulted, and vary in their degree of preservation of primary sedimentary structures. Commonly, small-scale folds are detached and randomly orientated. Large-scale folded strata can show stronger vergence directions.

and

ii. Clasts and megaclasts: Blocks of remobilized strata, varying in size, degree of disaggregation, and preservation of primary sedimentary structures. Clasts vary in scale from 10 cm diameter to 60 m thick and 750 m in length. Clasts are fractured and disaggregated at their edges with brittle deformation features. Smaller clasts are present within a matrix. Commonly, clasts comprise FA3 (Collingham Fm.) with minor amounts of FA2 (Whitehill Fm.).

Interpretation

i. Folded strata are interpreted to form through ductile deformation during remobilization of primary bedding and transport in slumps. The variety of fold sizes, attitudes, interlimb angles and primary bedding preservation is a result of the lithology, amount of consolidation prior to remobilization, and transport distance.

ii. Clasts and megaclasts are interpreted to be entrained at the headwall of the primary flow, or entrained from the underlying substrate and collapsing lateral margins during transport. Brittle deformation and preserved structures indicate lithification prior to entrainment. Large clasts are transported as slide blocks. Disaggregation at edges of clasts is interpreted to form during collision with other debris during transport.

STRATIGRAPHIC SUBDIVISION AND CORRELATION

The stratigraphic architecture is constrained using the two marker units described in the Methodology section (Fig. 3). The physical stratigraphy is also sub-divided by two large-scale erosion surfaces 1 and 2 (Fig. 3), which were walked out and identified by abrupt facies changes where underlying strata are truncated and overlying strata thin, fine and onlap the surface. The depositional architecture can be constrained by the dip of the strata below, outside, and above the interval of interest. Mean lithology, and in particular the proportion of clay, inside and outside the two main erosional, confining surfaces, Surface 1 and 2, are similar, and therefore the surface morphology and architecture of infilling stratal packages is unlikely to have been substantially altered by differential compaction.

Depositional architecture and facies distribution

The stratigraphy of the outcrop has been subdivided into 5 depositional packages (Figs 3 and 5).

Package 1

The base of Package 1 (P1, Fig. 5) comprises >50 m of Lower Ecca Group stratigraphy, including the upper Prince Albert Fm. (FA1; Fig. 4A), the Whitehill Fm. (FA2; Fig. 4B), and the Collingham Fm. (FA 3; Figs 4C, 4D, 4E and 4F). Palaeocurrent measurements from ripple lamination indicate eastward palaeoflow (Fig. 5). This basal section is overlain by a 25-30 m thick unit of thin siltstone turbidites with subordinate sandstone beds (FA 4), and intercalated small-scale (1-2 m) slumps that comprise siltstone beds (FA 6i; Fig. 6). The overlying 15-30 m thick unit comprises slumps (FA 6i) with a debrite matrix (FA 5) with minor basal incision (a few metres deep) that marks an uneven basal contact, although no large-scale erosional confinement is observed (Figs 6 and 7A). A 20 m thick and >100 m exposed outcrop length megaclast (FA 6ii) of Collingham Fm. (FA 3) (Fig. 5) is present at the top of this unit. Package 1 is in place east and west of the outcrop (Fig. 2B and 2C), but is locally cut-out by Surface 1 (Figs 5 and 7A).

Surface 1

Surface 1 (S1, Fig. 5) cuts down from the SE to the NW of the outcrop (Figs 5 and 7A) with an averaged compacted gradient of 8°. The width of this surface is 2.0-4.5 km with a depth of >90 m. In the SE, the surface initially incises the sand-rich folded strata in the upper part of Package 1, forming a sharp and smooth erosional contact (Fig. 7A). The surface is less distinct where it incises the underlying siltstone-rich sediment. Instead, a zone with an intense shear fabric up to 10 m thick is present that comprises small-scale (2-3 m thick/2-10 m long) sheath folds and low angle faults with varied orientations and displacement of 0.01-1 m (Fig. 8A). Shear zone sediments consist of lenticular packages of highly deformed and foliated siltstone and sandstone with no internal sedimentary structures (Fig. 8A). The lower part of this surface is inferred by thinning of the overlying deposits and truncation of underlying beds. To the NW, this surface passes into the subcrop, such that the deepest point of erosion is not exposed (Fig. 3).

Package 2

The base of Package 2 (P2, Fig. 5) is confined by Surface 1. In the NW of the outcrop, at its deepest exposed point, Surface 1 is overlain by a >60 m thick section of folded sandstone (FA 6i) with a debrite matrix (FA 7) (Figs 4O and 7C), exposed for >1.5 km, and dipping into the subcrop (Fig. 3). Metre-scale folds are present throughout the unit with intense shearing and thrusts along steep planes. Fold attitude varies from upright to recumbent, with interlimb angles from isoclinal to open. Hinge line and bedding plane measurement of smaller folds appear to be distributed randomly with most detached and supported by a debritic matrix. The fold axis of a 50 m high isoclinal fold is orientated roughly E-W, with the pole to best fit girdle of bedding measurements also indicating an E-W orientation of the fold hinge line (Fig. 5). Sharply overlying this unit is a megaclast of Whitehill and Collingham formations (FA 6ii), 750 m in outcrop length and up to 60 m thick (Fig. 7C). Bedding plane measurements within the clast are at higher angles (10-20°) and different orientations to the surrounding in-place strata and the clast shows deformed edges. In the SE, Package 2 comprises fine and medium sandstone packages 0.5-2 m thick, interbedded with thin bedded siltstone packages <0.5 m thick, which onlap Surface 1 (Fig. 3A).

Package 3

The lowermost strata of Package 3 (P3, Fig. 5) onlaps Surface 1, and comprises thick turbidite beds (FA 4) (Fig. 7A). Basal beds thicken and thin (0-2 m thick) over 10s of metres, and onlap the underlying megaclast at high angles (Figs 7A and 7B). Bedding orientations vary across the package, with an increase in dip from an average of 0-5°N centrally over the megaclast (Fig. 7B) to 20°-30° NNE towards the SE of the outcrop where the package onlaps Surface 1 (Fig. 7A). Ripple palaeocurrents show a large variation in direction (Fig. 5). An overlying 16-18 m thick package of thin bedded (1-10 cm thick) planar and rare ripple laminated sandstone turbidites (FA 4) (Fig. 3), interbedded with thin siltstone beds (<1 cm-2 cm) contains rare small-scale slumps (0.2-4 m thick). These lower two packages are cut out by Surface 2 to the NW. Overlying these thin bedded sandstones is a discontinuous 18-20 m package of small scale slumps (FA 6i; 0.2-4 m thick) interbedded with laminated siltstone (FA 4) and a further 10-12 m package of thin bedded siltstone with rare, thin (< 10 cm) sandstone beds (FA 4). Both packages onlap Surface 1 to the SE (Fig. 7A) and are eroded by Surface 2 to the NW (Fig. 5).

In the SE, the overlying 2-4 m thick package comprises thickly bedded fine- and medium-grained sandstone turbidites (FA 4) with NW and NE flute and groove palaeocurrents (Fig. 5). This is overlain by 3-5 metres of laterally continuous thin bedded (<1-3 cm) coarse siltstones and fine sandstones (FA 4). Beds have sigmoidal shapes and are moderately bioturbated. Overlying this is a package (up to 40 m thick) of fine and medium sandstone beds, which comprises structureless amalgamated beds with dewatering structures and some intercalated debrites and folded strata (FA 5 and 6i). The unit becomes more slump and debrite dominated as it thickens to the SE of the outcrop (Figs 8B, 8C and 8D), and dissected by numerous extensional faults with throws of cm to 10 m and displacement to the N and E (Fig. 7A).

Surface 2

Surface 2 (S2, Fig. 5) cuts down from the SE to the NW across the outcrop (Fig. 7) with an estimated compacted gradient of 4°. The surface is 2.0-4.5 km wide and >60 m deep. In the SE of the outcrop, where the surface cuts the sandstone-rich strata of upper Package 3, the surface is sharp with a stepped character (Figs 7A, 8B, 8C and 8D). Here, the surface is cut by numerous small scours that are 10s of cm wide and long and up to 15 cm deep (Figs 8E and 8F), with palaeocurrents to the E (Fig. 5). The scours are draped with mudstone clasts and coarser grained sand (medium sandstone) lag deposits (Figs 8E and 8F). Towards the centre of the outcrop where Surface 2 cuts through Package 3 fine grained chaotic facies, the surface becomes less distinct and forms a shear zone up to 6 m in thickness (Fig. 3). In the shear zone, beds are tightly folded and displaced (0.01-10 m) by faults. Further NW, the location of Surface 2 is expressed as a sharp, locally erosive contact between underlying and overlying debrites (Figs 7B and 7C).

Package 4

Package 4 (P4; Fig. 5) consists of debrites with highly disaggregated Collingham Fm. clasts (FA 6ii), from m to 10s of m in length and 1-10 m in thickness (FA 6ii) supported by a fine siltstone matrix, onlapping Surface 1 and locally thickening in lows (FA 5; Figs 3, 5, 6 and 8D). In the central area and NW of the outcrop, the lower package comprises debrites. Individual debrites comprise mm to cm diameter angular mudstone clasts and metre-scale folded sandstone beds (FA 6i) supported by a poorly sorted siltstone to fine sandstone matrix (FA 5) with clasts of bedded sandstone and coarse siltstone up to 20 m thick and 100 m in outcrop length (Figs 3, 7B, 7C and 9). This package of debrites thins and onlaps onto Surface 2 to the southwest. Overlying this is a unit of slumped and folded strata (FA 6i) (1-13 m in thickness), with some preservation of primary sedimentary structures (originally <1-2 cm thin bedded sandstones and siltstones, similar to Package 3 strata) in the central section of the outcrop (Fig. 7B) and small-scale extensional faulting (mm-20 cm throw) prevalent throughout with material down-stepping towards the SE. This passes into poorly sorted sandstone (FA 5) in the NW of the outcrop, which founders up to 5 m into the debrite below (Figs 7C and 9) and onlaps onto Surface 2.

Package 5

The basal section (22-32 m thick) of Package 5 consists of 0.3-2 m thick normally graded turbidite beds with thick siltstone caps (FA 4), interbedded with thinly laminated fine siltstone (FA 4) (0.1-4 m thick) (Fig. 9). Commonly, sandstone beds are planar laminated, with rare ripple laminations. Ripple palaeocurrents throughout this basal section are towards the E or W (Fig. 5). Package 5 thins to the SE (6-10 m thick) and onlaps Surface 2 (Fig. 7A). The basal section of Package 5 is overlain by a 2-4 m thick, laterally extensive debrite (FA 5) that comprises siltstone and fine sandstone, with extensive mm to cm diameter mudstone clasts throughout (Fig. 9). The debrite is overlain by another turbidite unit consisting of interbedded sandstone and siltstone beds with mudstone caps decreasing stratigraphically (FA 4) (Fig. 9). Beds contain mudstone clasts and organic matter at bed tops. Rare ripple and climbing ripple laminations are present, with a laterally traceable 0.5-1 m thick climbing ripple laminated bed with palaeocurrents generally towards the N but with a wide dispersal pattern (Fig. 5). This unit thins from 12 to 4 m from NW to SE, and onlaps Surface 2 to the SE (Figs 5 and 7A). Overlying this is a 3-5 m thick unit that comprises folded and dewatered sandstone beds (FA 6i) in a siltstone matrix (FA 5; Figs 4N, 7A, 7B and 9) that thins over thicker Package 3 deposits in the SE (Fig. 5). Overlying this is a laterally continuous turbidite unit (15 m thick) that is uniform across the section and is used as an upper datum, with flute and groove palaeocurrents to the NW, and ripple palaeocurrents N-W (Figs 3, 4i, 4G, 7A, 7B and 9).

Evolutionary model

Palaeocurrent measurements and the wider stratigraphic context of the outcrop, in combination with the sedimentary architecture and facies, have enabled the formation of an evolutionary model (Figs 5 and 10).

Package 1

Lower Ecca Group deposits present throughout the Karoo Basin are interpreted as basin floor deposits (e.g. Visser 1979; Oelofsen, 1987), with their uniform nature suggesting little to no seabed topography (P1i, Fig. 10). The large-scale debrite overlying the Lower Ecca Group strata with no confining erosion surface (Fig. 6) suggest that that they were unconfined in a downslope area, having outrun their basal shear surface onto the lower slope/basin-floor (e.g. Frey-Martinez *et al.,* 2006; Posamentier & Martinsen, 2011) (P1ii; Fig. 10). The megaclast is interpreted as a rafted block, and the origin from basin floor strata indicates a period of uplift/tilting of the southern basin margin to allow up-dip entrainment (P1ii; Fig. 10). Megaclasts carried within the debrite may have moved to the top due to kinetic sieving (Middleton & Hampton, 1976) or moved as slide blocks (Gee *et al.,* 2006).

Surface 1

Surface 1 (S1, Fig. 10) is interpreted as a basal shear surface varying laterally to a basal shear zone, overlain by a thick debrite that was either involved in the formation of the surface or emplaced later. The depth of erosion indicates a location on the submarine slope. The change noted in the nature of the surface, from a sharp erosional surface to a zone of intense shearing, coincides with the change in material from thickly bedded sandstone to thin-bedded siltstone (Figs 3 and 7A). The shear zone indicates that in the finer deposits strain was accommodated along multiple failure planes. The deformation along the basal shear surface or zone may have formed in the initial emplacement event, or been a protracted record of deformation (e.g. Alves & Lourenço, 2010). The overall thickness of the succession, and therefore the original depth of Surface 1 incision and the gradient of the basal shear surface and shear zone will have been reduced by burial and compaction.

Package 2

The axis of folds in slumps is thought to originate parallel to sub-parallel to the strike of the slope (Bradley & Hansen, 1998) therefore indicating the gross transport direction (Woodcock, 1979; Farrell, 1984; Farrell & Eaton, 1987). Bedding and hinge line measurements taken from large-scale fold structures in the lower slumped unit suggest a N or S movement direction if this is an attached structure and not a clast (Fig. 5). The range of sediments, types of deformation and presence of shear surfaces and thrusts indicate several sources and methods of transport of the debrite and slump deposits. The presence of megaclasts of the Collingham and Whitehill formations suggest that updip these strata had been tilted sufficiently to be entrained in the headwall or from the substrate by overriding mass flows (S1 & P2, Fig. 10). These infilling strata may represent: i) the failed material that was involved in the initial mass flow that formed the basal shear surface, ii) later infilling deposits (e.g. Laberg *et al.,* 2014), or iii) a combination of both (Ogiesoba & Hammes, 2012).

Package 3

Deposition of Package 3 marks the change to turbiditic strata (P3i, Fig. 10). Beds onlap topography created by the megaclast in the NW and Surface 1 in the SE. The widely dispersed palaeocurrents in the lower section of Package 3 (Fig. 5) indicate turbidity current deflection and reflection off erosional and depositional relief (e.g. Baines, 1984; Edwards *et al.,* 1994; Haughton, 1994; Kneller & McCaffrey, 1999; Jackson & Johnson, 2009). The thin normal grading of lower Package 3 turbidites suggests that the flows were weakly confined downdip. The thick, tabular sand-rich strata in the SE are interpreted as a lobe complex (*sensu* Deptuck *et al.,* 2008; Prélat *et al.,* 2009) that onlaps Surface 1 in the SE of the outcrop (P3ii, Fig. 10). Palaeocurrents at the base of the lobe complex have a more consistent direction to the NE, indicating less topographic influence than deposits below (Fig. 5). The consistent thick bedded sandstone packages suggest axial lobe deposits with a highly aggradational stacking pattern. The aggradational stacking and the absence of graded bed tops and lack of fines suggest downstream flow-stripping (Sinclair & Tomasso, 2002) within a 3D confining topography, similar to intraslope lobe complexes (Spychala *et al.,* 2015). Higher-density and coarser portions of flows are confined by a downstream topographical barrier, while low-density and finer portions of flows are able to breach this barrier and continue down-dip. The lobe complex is highly deformed with extensive soft-sediment deformation and shear failure surfaces in the SE of the outcrop, likely a result of instability after deposition above the lateral margin slope. Post-depositional tilting of this entire package is evident from the increased angle of bed dips (on average 20°) towards the basal shear surface/zone (Fig. 7A and 7B).

Surface 2

Surface 2 is interpreted as a second basal shear surface varying laterally to a basal shear zone (S2, Fig. 10). Variation in the character of the shear surface to zone is coincident with lithological variation in the eroded material. The surface is sharp and stepped where eroded into the lobe complex sandstones. The presence of numerous scour features as well as overlying mudstone clasts and coarse sediment lags indicate that, at least over the lobe deposits, the surface was exposed and formed a sediment bypass zone (*sensu* Stevenson *et al.,* 2015) prior to infill. In the central area, a zone of intense shear formed indicating that in the finer deposits strain was accommodated along multiple failure planes. This deformation may have formed in the initial emplacement event, or be a protracted record of deformation during infill (e.g. Alves & Lourenço, 2010).

Package 4

The debritic units represent the initial remobilized infill of Surface 2, onlapping and infilling in topographic lows. The direction of transport is unknown due to the degree of disaggregation, but may represent shedding of material from unstable margins or from an unstable headwall area (P4, Fig. 10). The recognition of thin bedded strata in the central area similar to that in the underlying Package 3 turbidites, and syn-sedimentary faulting, suggests the source of this material was from the substrate at the margin.

Package 5

Beds initially onlap topography created by underlying debrites (Package 4) and Surface 2 with palaeocurrents indicating reflection and deflection of turbidity currents (e.g. Edwards *et al.,* 1994) (P5i, Fig. 10). The thick, normal graded nature of turbidites suggests down-dip flow confinement that formed transient ponded accommodation. Laterally extensive debrites indicate continued slope instability and failure sourced from the headwall and/or lateral margins (P5i, Fig. 10). The transitional package (Fig. 9) marks the change from thick, normally graded beds to thinner, sharp topped beds with climbing ripple laminated beds, suggesting rapid decrease in flow confinement (e.g. Jobe *et al.,* 2012; Morris *et al.,* 2014). The thinning of the upper slumped layer over the lobe complex may indicate remnant Surface 2 topography, or may be a product of differential compaction during early burial (e.g. Alves, 2010). Deposition of the sharp-topped sandstone and siltstone beds of the uniform datum package is interpreted to represent the healing of the basal shear surface (P5ii, Fig. 10) when the flows were unconfined, with more consistent NE palaeocurrents.

DISCUSSION

Evolution of surfaces

The large scale, concave shape and gradient of basal shear surfaces documented indicates locations at the margins of the submarine landslides, with extensional structures signifying either the headwall or lateral margin. Indicators of transport direction include: bedding and hinge line measurements taken from large-scale fold structures in Package 1 suggesting N or S movement; Package 3 flute and groove measurements indicating NE palaeoflow; Surface 2 scours indicating E palaeoflow; and, Package 5 flute and groove measurements indicating NW to NE palaeoflow. In addition, the presence of an uplifting lateral basin margin to the south of the outcrop, and regional palaeocurrent and thickness trends (van der Merwe *et al*., 2014), support failure directions towards the north. Therefore, these basal shear surfaces are orientated sub-parallel to the direction of palaeoflow and are interpreted as lateral margins (Bull *et al.,* 2009; Alves, 2015) rather than headwalls.

Basal shear surfaces have been shown to be highly variable in their degree of substrate entrained, depth of incision, and changes in flow dynamics (e.g. Frey-Martinez *et al.,* 2006; Bull *et al.,* 2009; Alves & Lourenço, 2010; Laberg *et al.,* 2016; Ortiz-Karpf *et al*., 2017a). The primary morphology of a basal shear surface or zone is further complicated by post depositional remobilization, occurring directly after deposition on unstable gradients and/or due to differential compaction, especially over variably lithified substrate (Alves & Lourenço, 2010). Outcrop observations help to constrain where the character of the basal shear surface or zone can be attributed to shearing at the time of emplacement or secondary failure and compaction.

The thickness of a basal shear zone is in part controlled by the character of the sheared strata, the relative density/ thickness of the flow, the mode of transport (Alves & Lourenço, 2010), and the longevity of the movement. This study documents a clear association between the lithology of eroded material and the nature of the basal shear surface or zone (Fig. 11). Sharp, stepped surfaces occur when eroding into thickly bedded sandstone (Figs 8 and 11) and several-metre thick shear zones form where eroding into chaotic deposits/thinly bedded siltstone (Figs 7A and 11). The characteristics of the flow(s) that formed the initial basal shear surface or zone are unknown, and may be responsible for some of the spatial variations in the thickness and morphology of the basal shear zone, and the transition to a basal shear surface.

The formation of the basal shear surface was likely time transgressive, with initial failure along a single, or multiple closely spaced slip-planes, which deepened and widened. These changes in width and depth may have occurred through deformation and entrainment of the underlying substrate (van der Merwe *et al.,* 2009, 2011; Dakin *et al.,* 2013), plucking of clasts (Pickering & Corregidor, 2005; Eggenhuisen *et al.,* 2011) and faulting and collapse of lateral margins (Bull *et al*., 2009). The modification of the basal shear surface results from entrainment of large volumes of substrate (e.g. Dykstra *et al*., 2011; Dakin *et al.,* 2013). Therefore the material deposited downdip is a combination of the initially failing substrate and material collected during travel and varies greatly down the pathway of the flow (e.g. Piper *et al*., 1997; Gee *et al.*, 2006; Alves & Cartwright, 2010).

Post formation, secondary failures along the basal shear surface or zone are documented in the form of debrite packages overlying basal shear surfaces (Package 4), extensional faulting towards the SW in the central area (Package 3) and towards the N and E at the lateral margin (Package 4), and remobilization of the lobe complex (Package 3) (Fig. 7A). Downthrow was away from lateral margins and formed due to later deposition on an unstable gradient (Fig. 11). The unusual geometries and variation in dip across Package 3 (Figs 7A, 7B and 11) may be a factor of post deposition movement: i) directly after deposition, ii) later due to loading and/or differential compaction prior to erosion by Surface 2, or iii) later after the deposition of the entire succession. Differential compaction can be shown to have had an impact over the megaclast, which was lithified prior to deposition, therefore forming a topographic high (e.g. Alves, 2010). Post-depositional tilting is observed in the package overlying the megaclast due to the lithified megaclast compacting less than the laterally equivalent substrate. The increased angle of bedding dip (on average 20°) towards the lateral margins of the basal shear surface/zone (Figs 7A, 7B and 11), and stratigraphic decrease suggests that there was incremental post-depositional movement of strata above the basal shear surface (Fig. 11).

Palaeocurrent indicators from deposits directly overlying Surfaces 1 and 2, suggest different failure directions (Fig. 5). These two surfaces may represent two unrelated events, or represent different slip planes within a single landslide complex. Infill of Surface 1 prior to erosion by Surface 2 indicates several depositional episodes rather than different phases of the same event, similar to the Hinlopen Slide (Vanneste *et al.,* 2006) or the Sahara Slide Complex (Li *et al*., 2017). If Surface 1 and 2 represent the basal shear surfaces that coalesce updip into the headwall of a larger slide this could be characteristic of retrogressive erosional events (Piper *et al.,* 2012). If distinctly separate events, the initial failure event that formed Surface 1 may have removed deposits at the toe-of-slope, subsequently rendering the slope gradient unstable up-dip.

The sizes and dimensions of the basal shear surfaces or zones are similar to large-scale confining surfaces within entrenched slope valley systems (e.g. Posamentier & Kolla, 2003; Beaubouef, 2004; Hubbard *et al.,* 2009; Hodgson *et al.,* 2011). Channel systems can be partially infilled with debrites (e.g. Posamentier & Kolla, 2003), but do not contain the ponded turbidites noted in this study.

Erosional channel complexes are usually characterised by large scale, composite stepped surfaces formed by several stages of erosion (Campion *et al.,* 2000; Sprague *et al.,* 2002) and the stacking of component channels, and channel complexes (e.g. Macauley & Hubbard, 2013) and internal levee successions (Kane & Hodgson, 2011). These components are not present in this example.

Confinement styles

In this example, it is evident that >100 m of slope accommodation was formed as a result of substrate entrainment and emplacement of three large submarine landslides. A single landslide is characterised here by the possible formation of a single basal shear surface or zone, overlain by multiple slumps and debris flows with remnant topography infilled by remobilized deposits and turbidites. Variations in flow confinement can occur at m-to 10s of metres scale above relief on upper surfaces of remobilized units (Armitage *et al.,* 2009; Jackson & Johnson, 2009; Kneller *et al.,* 2016). Flow confinement can also occur at a larger scale (10s-100 m), above basal shear surfaces when a large frontal ramp is formed during the erosion and/or as a result of remobilized deposits forming a topographical barrier down-dip (Frey-Martinez *et al.,* 2006; Moernaut & De Batist, 2011; van der Merwe *et al*., 2011; Alves, 2015). Here, we consider both the confinement of initial remobilized deposits (formed during failure or deposited immediately after) within the basal shear surface, as well as the confinement of later turbidites/remobilized deposits (Figs 12 and 13).

The gradient and height of the lateral margins allowed full to partial confinement of flows within the basal shear surface or zone. Bed architecture and palaeocurrent indicators from overlying turbidites indicate that although reflection and deflection of flows (e.g. Kneller *et al*., 1991; Kneller & McCaffrey, 1999) were caused by rugose top surfaces of remobilized deposits infilling the basal shear surface/zone, no large scale deflection or reflection is documented away from the lateral margin, with flow largely moving parallel to the margin.

Three discrete stages of topography-controlled evolution are recognised. Stage 1 (Fig. 12) involves the deposition of large-scale unconfined slumps, slides and debrites, sourced from an uplifting tilted southern basin margin, but not contained by a basal shear surface. Stage 2 (Fig. 12) includes the formation of Surface 1 with steep lateral margins and initial infill of 60 m of thick, sand rich remobilized deposits. This package is overlain by onlapping turbidites and a lobe complex, with a stacking pattern and sand-rich nature that suggests weak down-dip confinement. Stage 3 (Fig. 12) includes the formation of a less steep lateral margin to the basal shear surface that is overlain by thinner debritic deposits and a turbiditic infill with a distinct change from thick well graded and onlapping beds to sharp topped laterally continuous beds, which supports a transition from confined (ponded) to unconfined deposition. Previous models have classified the remobilized infill above a basal shear surface into two end member scenarios: *frontally emergent* where deposits have outrun the basal shear surface onto the seabed, or *frontally confined* where topography downslope results in the ponding of remobilized deposits within basal shear surface accommodation, restricting outflow onto the seabed (Frey-Martinez *et al.,* 2006; Moernaut & De Batist, 2011). Factors determining the confinement style of landslides are the shape of the slope profile (controlling the headwall height, depth of incision and location of frontal ramp), the gradient of the slope (controlling the length of the slope section and the height drop of the basal shear surface) and the geotechnical properties of the substrate (e.g. Moernaut & De Batist, 2011).

Stage 1 (Fig. 12) deposits can be classified as part of a frontally emergent landslide (*sensu* Frey-Martinez *et al.,* 2006) with its corresponding basal shear surface located up-dip of the outcrop (Figs 12 and 13A). Stage 2 (Fig. 12) shows evidence of partially graded turbidites overlying thick remobilized deposits, suggesting weak down-dip confinement. This supports deposition behind a frontally confined landslide (*sensu* Frey-Martinez *et al.,* 2006) (Figs 12 and 13A). Similarly, in Stage 3 (Fig. 12) thick graded turbidites indicate either a section of a frontally confined landslide with down-dip confinement formed by a frontal ramp on the basal shear surface, or a frontally emergent landslide with the MTC infill forming a topographical barrier. The latter may be more likely as the remobilized infill of Surface 2 is relatively thin at the outcrop location and therefore a large proportion may have bypassed down-dip (Figs 12 and 13A). Moreover it is not possible to resolve whether the remobilized deposits infilling the surface were those involved in the original landslide, although this relationship is commonly invoked from stratal relationships in 3D reflection seismic data (e.g. Posamentier & Kolla, 2003; Posamentier & Martinsen, 2011; Ortiz-Karpf *et al*., 2017a).

The formation of a landslide as frontally emergent or frontally confined will greatly affect the amount and location of onlapping and ponded infill. Frontally emergent landslides will likely leave larger evacuated depressions with down-dip confining topography, within which thick packages of turbidites and remobilized deposits can aggrade (e.g. Stage 3). In addition, surface ponding of flow will occur on top of the rugose surface of the emergent remobilized deposit when up-dip accommodation is healed (e.g. Stage 1). Frontally confined landslides will have a complex rugose top surface, with localised depressions infilled with turbidites and remobilized deposits, but likely contain comparatively thinner infilling packages. Therefore, it is more likely that Stage 2 and 3 deposits also represent frontally emergent landslides and subsequent infill but with increasing amounts of seabed topography, resulting in increased flow confinement.

Moernaut & De Bastist (2011) suggested that an increase in slope gradient, such as that documented by uplift/tilting of the basin margin in this study, may result in more frontally emergent (unconfined) landslides forming due to reduced static and kinetic friction along the basal shear surface and therefore more efficient potential energy transfer. Although this may only be the case when considering individual landslides, due to the multiphase nature of the succession, the stacking of multiple remobilized deposits downslope will result in a higher down-dip topographic barrier forming through time, which would require more gravitational potential energy to overcome. The increase in slope gradient will create a progressively more out-of-phase slope profile, possibly resulting in increased basal shear surface depths within subsequent landslides, leading to more frontal confinement (Frey-Martinez *et al.,* 2006; Moernaut & De Batist*,* 2011). The properties of the material in which the failure occurred is thought to influence slope stability, with failures within rheologically stronger material being smaller and more deep-seated than those in weaker material, typically resulting in a steeper post-failure slope (McAdoo *et al.,* 2000). Therefore, successive failures progressively evacuating deeper and more consolidated material may create smaller, more confined landslides. Although landslides likely remained 'unconfined' within this study due to the factors discussed above, initial remobilized infill may have become relatively more 'confined' with shorter run-out distances, and therefore creating more 3D topographic closure, resulting in increased confinement of later turbidite and remobilized infill (Figs 13A and 13B).

Regardless of whether down-dip confining topography was created by a frontal ramp in the basal shear surface or mounded mass flow deposits, there is a clear signature of increasing confinement within the turbiditic infill from Stage 1 to Stage 3 (Figs 12, 13A and 13B). This may be a natural evolution for multiphase failures on steepening/lengthening slopes (Fig. 13B), which occur globally and have been widely documented, including in ancient tectonically controlled settings (Alves & Lourenço, 2010), related to salt withdrawal (Ogiesoba & Hammes, 2012) and modern volcanic islands (Carracedo *et al.,* 1999; Urgeles *et al.,* 2001). Therefore, this model is applicable to both modern and ancient multiphase submarine landslides in many geographical locations.

Source slope

The large scale and deeply erosional basal shear surfaces with infilling deposits recognised in this study are located in the distal, easternmost area of the Laingsburg depocentre (Fig. 2A). Palaeocurrent and sedimentological evidence suggests that they were not fed through the depocentre from the westerly dominant sediment transport direction (Flint *et al*., 2011; van der Merwe *et al*., 2014; Fig. 5). The material present infilling the landslides includes a large range of grain sizes, including medium-grained sandstone, which is unusually coarse for deposits in the Laingsburg system (Grecula *et al.,* 2003; Sixsmith *et al.,* 2004; Hodgson *et al.,* 2006; Hofstra *et al.,* 2015). This larger grain size and more northward trending palaeocurrents in the study area (Fig. 5) suggests that many of the infilling packages are more genetically related to the Ripon Fm. deposits present to the east around the Prince Albert area. Coupled with the interpreted north-facing basin margin that controlled later Fort Brown Fm. deposition (van der Merwe *et al.,* 2014), this suggests that the failure surfaces and much of the infilling strata originated from a lateral basin margin to the south. Although ponded deposits infilled the accommodation created by basal shear surfaces (Fig. 10), no long-term southerly sediment conduit has been documented. This suggests that the source slope of these failures was not a major supply margin to the basin at this point, rather an actively uplifting lateral confining slope.

Sedimentation rates vs. degradation rates

Many studies have shown how submarine landslides can capture/reroute sediment pathways (e.g. Loncke *et al.,* 2009; Ortiz-Karpf *et al.,* 2015) and pond flows (e.g. Alves & Cartwright, 2010; Kneller *et al.,* 2016). These studies are examples of slope failures in locations with high sediment input, such as directly down-dip of delta fronts (Fig. 14). The loading caused by high sediment input may be a controlling factor in causing failure in these locations. These features can be healed quickly where sedimentation rates are higher than degradation rates. Conversely slope failure can also occur in areas of little sediment input, with only passive, hemipelagic infill or infill by sporadic flows/bottom currents, such as on non-supply margins or salt/mud diapir controlled topography (e.g. McAdoo *et al.,* 2000). In these locations, the degradation rate of the slope greatly outpaces the sedimentation rate. The stacked landslide complex outlined in this study clearly has episodic coarse sediment infill but also shows evidence of periods with low rates of sedimentation. There is no evidence of large-scale, long-term sediment bypass in the form of channel complexes. It is also unknown if Surface 1 became completely filled and overspilled prior to the erosion of Surface 2. Overall, the sedimentation rate was in balance with the degradation rate throughout most of the system evolution. It is possible that these failures occurred in the periphery of an area of sediment input to create these changing conditions, for example capturing flows transported across the shelf/upper slope feeding the Ripon system to the east but unable to re-route entire slope systems (Fig. 14). The model presented in Figure 14 demonstrates how wider scale knowledge of the basin, which is often lacking in outcrop studies, can be gained from general characterisation of landslide infill.

CONCLUSIONS

This study documents an exceptionally well-exposed example of the formation, evolution and infill of multiple seismic-scale, submarine landslides. Two 2.0-4.5 km wide basal shear surfaces/zones, Surface 1 and 2, are interpreted as rare examples of lateral margins commonly identified in subsurface data. Surface 1 and 2 document minimum evacuation depths of 90 m and 60 m, with compacted lateral gradients of 8° and 4°, respectively. The basal shear surfaces display variation across strike, coincident with changes in lithology of eroded deposits. Sharp, distinct, commonly stepped surfaces formed where thick sand-rich deposits are eroded and are sometimes mantled with scours and bypass lags. Where these surfaces cut mud-rich deposits, shear zones up to 10 m thick developed, with evidence of protracted development likely due to oversteepening and weakening of material during erosion or after loading. The evolution of this submarine landslide complex can be divided into three stages: 1) unconfined deposition of slumps and debris flows that outran their basal shear surface; 2) erosion by basal shear surface 1, overlain by thick slumps and debrites and infilled by weakly confined turbidites and a lobe complex; 3) erosion by basal shear surface 2, overlain by thin debrites and infilled by confined turbidites that transition stratigraphically into unconfined turbidites. All three stages of failure are likely 'frontally emergent' landslides, with stacking of failed deposits down-dip. The progressive increase in down-dip topography caused a stratigraphic increase in confinement of turbidity currents. The failure source slope was likely a non-supply lateral basin margin that was actively tilting/uplifting, as evidenced by the entrainment of megaclasts from underlying basin-floor successions. Periods of high and low energy deposition are apparent, with only minor sediment bypass and no development of channels. Therefore, this landslide complex likely formed in a location with fluctuating sediment input, which over the timescale of the landslide complex, was comparable to the degradation rate.

The increase in confinement of remobilized deposits and turbidites, with stacking of landslides, may represent a model applicable to other failures on steepening/lengthening slopes. Moreover, the recognition of these submarine landslides in an area peripheral to the main sediment input highlights the necessity to consider wider basin sedimentation/degradation rates when assessing impact of slope failures on sediment routing, hydrocarbon reservoir connectivity, and seal potential.

Acknowledgements

The authors thank the local farmers of the Prince Albert area for permission to undertake field studies on their land. De Ville Wickens helped with regional context and logistical support. We thank Colleen Kurcinka, Sarah Cobain, Sophie Cullis and Grace Cosgrove for field assistance. This work was carried out as part of the SLOPE 4 consortium research project. We are grateful for financial support from: Anadarko, BHP Billiton, BP, ConocoPhillips, ENGIE, Maersk Oil, Murphy, Nexen, Petrobras, Premier Oil, Shell, Statoil, Total, VNG Norge and Woodside. The authors would also like to thank Tiago Alves, Sverre Henriksen, an anonymous reviewer, associate editor Jess Trofimovs, and chief editor Nigel Mountney for their insightful comments and helpful suggestions to improve the manuscript.

REFERENCES

Alfaro, E. and **Holz, M.** (2014) Seismic geomorphological analysis of deepwater gravity-driven deposits on a slope system of the southern Colombian Caribbean margin. *Marine and Petroleum Geology*, **57**, 294-311.

Allen, J.R.L. (1984) Parallel lamination developed from upper-stage plane beds: a model based on the larger coherent structures of the turbulent boundary layer. *Sedimentary Geology*, **39**, 227-242. doi: 10.1016/0037-0738(84)90052-6.

Alves, T.M. (2010) 3D Seismic examples of differential compaction in mass-transport deposits and their effect on post-failure strata. *Marine Geology*, **271**, 212-224.

Alves, T.M. (2015) Submarine slide blocks and associated soft-sediment deformation in deep-water basins: A review. *Marine and Petroleum Geology*, **67**, 262-285.

Alves, T.M. and **Cartwright, J.A.** (2010) The effect of mass-transport deposits on the younger slope morphology, offshore Brazil. *Marine and Petroleum Geology*, **27**, 2027-2036.

Alves, T.M. and **Lourenço, S.D.N.** (2010) Geomorphic features related to gravitational collapse: Submarine landsliding to lateral spreading on a Late Miocene- Quaternary slope (SE Crete, eastern Mediterranean). *Geomorphology*, **123**, 13-33.

Antobreh, A.A. and **Krastel, S.** (2007) Mauritania Slide Complex: morphology, seismic characterisation and processes of formation. *International Journal of Earth Sciences,* **96**, 451-472.

Armitage, D.A., Romans, B.W., Covault, J.A. and **Graham, S.A.** (2009) The influence of mass-transport-deposit surface topography on the evolution of turbidite architecture: the Sierra Contreras, Tres Pasos Formation (Cretaceous), southern Chile*. Journal of Sedimentary Research,* **79**, 287-301.

Baeten, N.J., Laberg, J.S., Forwick, M., Vorren, T.O., Vanneste, M., Forsberg, C.F., Kvalstad, T.J. and **Ivanov, M.** (2013) Morphology and origin of smaller-scale mass movements on the continental slope off northern Norway. *Geomorphology*, **187**, 122-134.

Baeten, N.J., Laberg, J.S., Vanneste, M., Forsberg, C.F., Kvalstad, T.J., Forwick, M., Vorren, T.O. and **Haflidason, H**. (2014) Origin of shallow submarine mass movements and their glide planes—Sedimentological and geotechnical analyses from the continental slope off northern Norway. J*ournal of Geophysical Research: Earth Surface,* **119**, 2335-2360.

Baines, P.G. (1984) A unified description of two-layer flow over topography. *Journal of Fluid Mechanics,* **146**, 127-167.

Beaubouef, R.T. (2004) Deep-water leveed-channel complexes of the Cerro Toro Formation, Upper Cretaceous, southern Chile. *AAPG Bulletin*, **88,** 1471-1500.

Bellaiche, G., Coutellier, V. and **Droz, L.** (1986) Seismic evidence of widespread mass transport deposits in the Rhône deep-sea fan: their role in the fan construction. *Marine Geology*, **71**, 327-340.

Best, J. and **Bridge, J.** (1992) The morphology and dynamics of low amplitude bedwaves upon upper stage plane beds and the preservation of planar laminae. *Sedimentology*, **39**, 737-752.

Bouma, A. (1962) Sedimentology of some flysch deposits. A graphic approach to facies interpretation. Elsevier, Amsterdam, 168 pp.

Bradley, D. and **Hanson, L.** (1998) Paleoslope analysis of slump folds in the Devonian flysch of Maine. *The Journal of Geology,* **106,** 305-318.

Buhmann, D., Buhmann, C. and **von Brunn, V.** (1989) Glaciogenic banded phosphorites from Permian sedimentary rocks. *Bulletin of the Society of Economic Geologists*, **48**, 741–750.

Bull, S., Cartwright, J. and **Huuse, M.,** (2009) A review of kinematic indicators from mass-transport complexes using 3D seismic data. *Marine and Petroleum Geology*, **26**, 1132-1151.

Callot, P., Sempere, T., Odonne, F. and **Robert, E.** (2008) Giant submarine collapse of a carbonate platform at the Turonian-Coniacian transition: The Ayabacas Formation, southern Peru. *Basin Research*, **20**, 333-357.

Campion, K.M., Sprague, A.R., Mohrig, D., Lovell, R.W., Drzewiecki, P.A., Sullivan, M.D., Ardill, J.A., Jensen, G.N. and **Sickafoose, D.K.** (2000) Outcrop expression of confined channel complexes. In: *Deep-water Reservoirs of the World* (Eds P. Weimar, R.M. Slatt, J. Coleman, N.C. Rosen, H. Nelson, A.H. Bouma, M.J. Styzen and D.T. Lawrence) *Gulf Coast Section Society of Economic Palaeontologists and Mineralogists*, 127-150.

Carracedo, J.C., Day, S.J., Guillou, H. and **Torrado, F.J.P.** (1999) Giant Quaternary landslides in the evolution of La Palma and El Hierro, Canary Islands*. Journal of Volcanology and Geothermal Research*, **94**, 169-190.

Catuneanu, O., Hancox, P.J. and **Rubidge, B.S.** (1998) Reciprocal flexural behaviour and contrasting stratigraphies: a new basin development model for the Karoo retroarc foreland system, South Africa. *Basin Research*, **10**, 417-439.

Dakin, N., Pickering, K.T., Mohrig, D. and **Bayliss, N.J.** (2013) Channel-like features created by erosive submarine debris flows: Field evidence from the Middle Eocene Ainsa Basin, Spanish Pyrenees. *Marine and Petroleum Geology*, **41**, 62-71.

Deptuck, M.E., Piper, D.J., Savoye, B. and **Gervais, A.** (2008) Dimensions and architecture of late Pleistocene submarine lobes off the northern margin of East Corsica. *Sedimentology*, **55,** 869-898.

Di Celma, C., Brunt, R.L., Hodgson, D.M., Flint, S.S. and **Kavanagh, J.P.** (2011) Spatial and temporal evolution of a Permian submarine slope channel-levee system, Karoo Basin, South Africa. *Journal of Sedimentary Research*, **81**, 579-599, doi: 10.2110/jsr.2011.49.

Domack, E.W. (1983) Facies of late Pleistocene glacial-marine sediments on Whidbey Island, Washington. In*: Glacial-marine Sedimentation* (Ed. B.F. Molnia), pp. 535-570. Plenum Press, New York.

Driscoll, N.W., Weissel, J.K. and **Goff, J.A.** (2000) Potential for large-scale submarine slope failure and tsunami generation along the US mid-Atlantic coast. *Geology*, **28**, 407-410.

Dykstra, M., Garyfalou, K., Kertznus V., Kneller, B., Milana, J.P., Molinaro, M., Szuman, M., and **Thompson, P.** (2011) Mass-transport deposits: combining outcrop studies and seismic forward modeling to understand lithofacies distributions, deformation, and their seismic stratigraphic expression. In: *Mass Transport Deposits in Deepwater Settings* (Eds. C. Shipp, P. Weimer and H. Posamentier). *SEPM, Special Publication* **96**, 293–310.

Edwards, D.A., Leeder, M.R., Best, J.L. and **Pantin, H.M.** (1994) On experimental reflected density currents and the interpretation of certain turbidites. *Sedimentology*, **41**, 437-461.

Eggenhuisen, J.T., McCaffrey, W.D., Haughton, P.D. and **Butler, R.W.** (2011) Shallow erosion beneath turbidity currents and its impact on the architectural development of turbidite sheet systems. *Sedimentology*, **58**, 936-959.

Fallgatter, C., Kneller, B., Paim, P.S.G. and **Milana, J.P.** (2017) Transformation, partitioning and flow–deposit interactions during the run-out of megaflows. *Sedimentology,* **64**, 359–387. Doi: 10.1111/sed.12307

Farrell, S.G. (1984) A dislocation model applied to slump structures, Ainsa Basin, South Central Pyrenees. *Journal of Structural Geology*, **6**, 727-736.

Farrell, S.G. and **Eaton, S.** (1987) Slump strain in the Tertiary of Cyprus and the Spanish Pyrenees. Definition of palaeoslopes and models of soft-sediment deformation. In: *Deformation of Sediments and Sedimentary Rocks* (Eds M.F. Jones and R.M.F Preston). *Special Publication of the Geological Society of London,* **29**, 181-196.

Flint, S.S., Hodgson, D.M., Sprague, A.R., Brunt, R.L., van der Merwe, W.C., Figueiredo, J., Prélat, A., Box, D., Di Celma, C. and **Kavanagh, J.P.** (2011) Depositional architecture and sequence stratigraphy of the Karoo basin floor to shelf edge succession, Laingsburg depocentre, South Africa. *Marine and Petroleum Geology*, **28**, 658–674. doi: 10.1016/j.marpetgeo.2010.06.008.

Frey-Martinez, J., Cartwright, J. and **Hall, B.** (2005) 3D seismic interpretation of slump complexes: examples from the continental margin of Israel. *Basin Research*, **17**, 83-108.

Frey-Martínez, J., Cartwright, J. and **James, D.** (2006) Frontally confined versus frontally emergent submarine landslides: a 3D seismic characterisation. *Marine and Petroleum Geology*, **23**, 585-604.

Gamberi, F., Rovere, M. and **Marani, M.** (2011) Mass-transport complex evolution in a tectonically active margin (Gioia Basin, Southeastern Tyrrhenian Sea). *Marine Geology*, **279**, 98-110.

Gee, M.J., Watts, A.B., Masson, D.G. and **Mitchell, N.C.** (2001) Landslides and the evolution of El Hierro in the Canary Islands. *Marine Geology*, **177**, 271-293

Gee, M.J.R., Gawthorpe, R.L. and **Friedmann, S.J.** (2006) Triggering and evolution of a Giant Submarine Landslide, Offshore Angola, revealed by 3D seismic stratigraphy and geomorphology. *Journal of Sedimentary Research*, **76**, 9-19.

Grecula, M., Flint, S., Potts, G., Wickens, D. and **Johnson, S.** (2003) Partial ponding of turbidite systems in a basin with subtle growth-fold topography: Laingsburg-Karoo, South Africa. *Journal of Sedimentary Research*, **73**, 603-620.

Haflidason, H., Sejrup, H.P., Nygård, A., Mienert, J., Bryn, P., Lien, R., Forsberg, C.F., Berg, K. and **Masson, D.** (2004) The Storegga Slide: architecture, geometry and slide development. *Marine Geology*, **213**, 201-234.

Hampton, M.A., Lee, H.J. and **Locat, J.** (1996) Submarine landslides. *Reviews of Geophysics*, **34**, 33–59.

Haughton, P.D. (1994) Deposits of deflected and ponded turbidity currents, Sorbas Basin, southeast Spain. *Journal of Sedimentary Research*, **64**, 233-246.

Herbert, C.T. and **Compton, J.S**. (2007) Depositional environments of the lower Permian Dwyka diamictite and Prince Albert shale inferred from the geochemistry of early diagenetic concretions, southwest Karoo Basin, South Africa. *Sedimentary Geology*, **194**, 263-277.

Hodgson, D.M., Flint, S.S., Hodgetts, D., Drinkwater, N.J., Johannessen, E.P. and **Luthi, S.M.** (2006) Stratigraphic evolution of fine-grained submarine fan systems, Tanqua depocenter, Karoo Basin, South Africa. *Journal of Sedimentary Research*, **76**, 20-40.

Hodgson, D.M., Di Celma, C., Brunt, R.L. and **Flint, S.S**. (2011) Submarine slope degradation and aggradation and the stratigraphic evolution of channel-levee systems. *Journal of the Geological Society*, **168**, 625-628. doi: 10.1144/0016-76492010-177.

Hoffman, J.S., Kaluza, M.J., Griffiths, R., McCullough, G., Hall, J. and **Nguyen, T**. (2004) Addressing the Challenges in the Placement of Seafloor Infrastructure on the East Breaks Slide-A Case Study: The Falcon Field (EB 579/623), northwestern Gulf of Mexico. *Offshore Technology Conference, Contribution 16748,* pp. 18.

Hofstra, M., Hodgson, D.M., Peakall, J. and **Flint, S.S.** (2015) Giant scour-fills in ancient channel-lobe transition zones: Formative processes and depositional architecture. *Sedimentary Geology*, **329**, 98-114.

Hubbard, S.M., de Ruig, M.J. and **Graham, S.A.** (2009) Confined channel-levee complex development in an elongate depo-center: deep-water Tertiary strata of the Austrian Molasse basin. *Marine and Petroleum Geology,* **26**, 85-112.

Hunt, J.E., Wynn, R.B., Talling, P.J. and **Masson, D.G.** (2013) Turbidite record of frequency and source of large volume (> 100 km^3) Canary Island landslides in the last 1.5 Ma: Implications for landslide triggers and geohazards. *Geochemistry, Geophysics, Geosystems*, **14**, 2100-2123.

Hürlmann, M., Martí, J. and **Ledesma, A.** (2004). Morphological and geological aspects related to large slope failures on oceanic islands: The huge La Orotava landslides on Tenerife, Canary Islands. *Geomorphology*, **62**, 143-158.

Jackson, C.A-L. (2011) Three-dimensional seismic analysis of megaclast deformation within a mass transport deposit; implications for debris flow kinematics. *Geology*, **39**, 203-206.

Jackson, C.A. and **Johnson, H.D.** (2009) Sustained turbidity currents and their interaction with debrite-related topography; Labuan Island, offshore NW Borneo, Malaysia. *Sedimentary Geology,* **219**, 77-96.

Joanne, C., Lamarche, C., and **Collot, J.-Y**. (2013) Dynamics of giant mass transport in deep submarine environments: the Matakaoa Debris Flow, New Zealand. *Basin Research*, **25**, 471–488

Jobe, Z.R., Lowe, D.R. and **Morris, W.R.** (2012) Climbing-ripple successions in turbidite systems: depositional environments, sedimentation rates and accumulation times. *Sedimentology*, **59**, 867-898.

Johnson, M.R., Van Vuuren, C.J., Visser, J.N.J., Cole, D.I., Wickens, H.D.V., Christie, A.D.M. and **Roberts, D.L** (1997) The foreland Karoo Basin, South Africa. In: *African Basins*: *Sedimentary Basins of the World,* (Ed. R.C. Selly), **3**, p. 269–317.Elsevier Science, Amsterdam.

Johnson, M.R., van Vuuren, C.J., Visser, J.N.J., Cole, D.I., Wickens, H.D., Christie, A.D.M., Roberts, D.L. and **Brandl, G.** (2006) Sedimentary rocks of the Karoo Supergroup, In: *The Geology of South Africa* (Eds M.R. Johnson, C.R. Anhaeusser and R.J Thomas) *Geological Society of South Africa and Council for Geoscience*, 461–499.

Jones, G.E.D., Hodgson, D.M. and **Flint, S.S.** (2015) Lateral variability in clinoform trajectory, process regime, and sediment dispersal patterns beyond the shelf-edge rollover in exhumed basin margin-scale clinothems. *Basin Research*, **27**, 657-680. doi: 10.1111/bre.12092.

Kane, I.A. and **Hodgson, D.M.** (2011) Sedimentological criteria to differentiate submarine channel levee subenvironments: exhumed examples from the Rosario Fm. (Upper Cretaceous) of Baja California, Mexico, and the Fort Brown Fm. (Permian), Karoo basin, S. Africa. *Marine and Petroleum Geology*, **28**, 807-823.

King, P.R., Ilg, B.R., Arnot, M, Browne, G.H., Strachan, L.J., Crundwell, M. and **Helle, K.** (2011) Outcrop and seismic examples of mass-transport deposits from a late Miocene deep-water succession, Taranaki Basin, New Zealand. In: *Mass-Transport Deposits in Deepwater Settings* (Eds R.G. Shipp, P. Weimer, H.W. Posamentier), *Society for Sedimentary Geology (SEPM) Special Publication,* **96**, 311-348.

Kingsley, C.S. (1981) A composite submarine fan-delta-fluvial model for the Ecca and lower Beaufort Groups of Permian age in the eastern Cape Province, South Africa. *Transactions of the Geological Society South Africa*, **84**, 27-40.

Kneller, B.C. and **Branney, M.J.** (1995) Sustained high-density turbidity currents and the deposition of thick massive sands. *Sedimentology*, **42**, 607-616. doi: 10.1111/j.1365-3091.1995.tb00395.x.

Kneller, B.C. and **McCaffrey, W.D**. (1999) Depositional effects of flow non-uniformity and stratification within turbidity currents approaching a bounding slope: deflection, reflection and facies variation. *Journal of Sedimentary Research*, **69**, 980-991

Kneller, B., Edwards, D., McCaffrey, W. and **Moore, R.** (1991) Oblique reflection of turbidity currents. *Geology*, **19**, 250-252.

Kneller, B., Dykstra, M., Fairweather, L. and **Milana, J.P.** (2016) Mass-transport and slope accommodation: Implications for turbidite sandstone reservoirs. *AAPG Bulletin*, **100**, 213-235.

Laberg, J.S., Kawamura, K., Amundsen, H., Baeten, N., Forwick, M., Rydningen, T.A. and **Vorren, T.O.** (2014) A submarine landslide complex affecting the Jan Mayen Ridge, Norwegian–Greenland Sea: slide-scar morphology and processes of sediment evacuation. *Geo-Marine Letters*, **34**, 51-58.

Laberg, J.S., Strasser, M., Alves, T.M., Gao, S., Kawamura, K., Kopf, A. and **Moore, G.F.** (2016) Internal deformation of a muddy gravity flow and its interaction with the seafloor (site C0018 of IODP Expedition 333, Nankai Trough, SE Japan). *Landslides*, **13**, 1-12.

León, R., Somoza, L., Urgeles, R., Medialdea, T., Ferrer, M., Biain, A., García-Crespo, J., Mediato, J.F., Galindo, I., Yepes, J. and **González, F.J.** (2017) Multi-event oceanic island landslides: New onshore-offshore insights from El Hierro Island, Canary Archipelago. *Marine Geology*, doi: 10.1016/j.margeo.2016.07.001.

Li, W., Alves, T.M., Urlaub, M., Georgiopoulou, A., Klaucke, I., Wynn, R.B., Gross, F., Meyer, M., Repschläger, J., Berndt, C. and **Krastel, S**. (2017) Morphology, age and sediment dynamics of the upper headwall of the Sahara Slide Complex, Northwest Africa: Evidence for a large Late Holocene failure. *Marine Geology*, DOI: 10.1016/j.margeo.2016.11.013.

Locat, J. and **Lee, H.J**. (2002) Submarine landslides: advances and challenges. *Canadian Geotechnical Journal*, **39**, 193-212.

Loncke, L., Gaullier, V., Droz, L., Ducassou, E., Migeon, S. and **Mascle, J.** (2009) Multi-scale slope instabilities along the Nile deep-sea fan, Egyptian margin: a general overview. *Marine and Petroleum Geology*, **26**, 633-646.

Lowe, D.R. (1982) Sediment gravity flows: II Depositional models with special reference to the deposits of high-density turbidity current. *Journal of Sedimentary Petrology*, **52**, 279–298.

Lucente, C.C. and **Pini, G.A.** (2003) Anatomy and emplacement mechanism of a large submarine slide within a Miocene foredeep in the northern Apennines, Italy: A field perspective. *American Journal of Science*, **303**, 565-602.

Løvholt, F., Harbitz, C.B. and **Haugen, K.B.** (2005) A parametric study of tsunamis generated by submarine slides in the Ormen Lange/Storegga area off western Norway. *Marine and Petroleum Geology*, **22**, 219-231.

Macauley, R.V. and **Hubbard, S.M.** (2013) Slope channel sedimentary processes and stratigraphic stacking, Cretaceous Tres Pasos Formation slope system, Chilean Patagonia. *Marine and Petroleum Geology*, **41**, 146-162.

Martinsen, O.J. (1989) Styles of soft-sediment deformation on a Namurian (Carboniferous) delta slope, Western Irish Namurian Basin, Ireland. In: *Deltas–Sites and Traps of Fossil Fuels* (Eds. M.H. Whateley and K.T. Pickering), *Geological Society, London, Special Publications*, **41**, 167-177.

Martinsen, O.J. (1994) Mass movements. In: *The Geological Deformation of Sediments* (Ed. A. Maltman). Chapman and Hall, London, pp. 127–165

Martinsen, O.J. and **Bakken, B.** (1990) Extensional and compressional zones in slumps and slides in the Namurian of County Clare, Ireland. *Journal of the Geological Society of London*, **147**, 153-164.

Masson, D.G., Watts, A.B., Gee, M.J.R., Urgeles, R., Mitchell, N.C., Le Bas, T.P. and **Canals, M.** (2002) Slope failures on the flanks of the western Canary Islands. *Earth-Science Reviews*, **57**, 1-35.

Masson, D.G., Harbitz, C.B., Wynn, R.B., Pedersen, G. and **Løvholt, F.** (2006) Submarine slides: processes, triggers and hazard prediction. *Philosophical Transactions of the Royal Society A*, **364**, 2009-2039. doi: 10.1098/rsta.2006.1810

Masson, D.G., Wynn, R.B. and **Talling, P.J.** (2010) Large landslides on passive continental margins: processes, hypotheses and outstanding questions. In: *Submarine Mass Movements and Their Consequences* (Eds. D.C. Mosher, C. Shipp, L. Moscardelli, J. Chaytor, C. Baxter, H. Lee and R. Urgeles), pp. 153-165. Springer, Netherlands.

McAdoo, B.G., Pratson, L.F. and **Orange, D.L.** (2000) Submarine landslide geomorphology, US continental slope. *Marine Geology*, **169**, 103-136.

McKay, M.P., Weislogel, A.L., Fildani, A., Brunt, R.L., Hodgson, D.M. and **Flint, S.S.** (2015) U-PB zircon tuff geochronology from the Karoo Basin, South Africa: implications of zircon recycling on stratigraphic age controls. *International Geology Review*, **57**, 393-410.

Middleton, G.V. and **Hampton, M.A**. (1976) Subaqueous sediment transport and deposition by sediment gravity flows. In: *Marine Sediment Transport and Environmental Management* (Eds. D.J. Stanley and D.J.P. Swift), pp. 197–218. Wiley, New York.

Moernaut, J. and **De Batist, M.** (2011) Frontal emplacement and mobility of sublacustrine landslides: results from morphometric and seismostratigraphic analysis. *Marine Geology*, **285**, 29-45

Morris, E.A., Hodgson, D.M., Brunt, R.L. and **Flint, S.S.** (2014) Origin, evolution and anatomy of silt-prone submarine external levees. *Sedimentology*, **61**, 1734-1763. doi:10.1111/sed.12114.

Moscardelli, L. and **Wood, L.** (2008) New classification system for mass transport complexes in offshore Trinidad. *Basin Research*, **20**, 73-98.

Moscardelli, L. and **Wood, L.** (2015) Morphometry of mass-transport deposits as a predictive tool, *GSA Bulletin,* **128**, 47-80. doi: 10.1130/B31221.1

Moscardelli, L., Wood, L. and **Mann, P**. (2006) Mass-transport complexes and associated processes in the offshore area of Trinidad and Venezuela. *AAPG Bulletin*, **90**, 1059-1088.

Mulder, T. and **Alexander, J.** (2001) Abrupt change in slope causes variation in the deposit thickness of concentrated particle-driven density currents. *Marine Geology*, **175**, 221-235. doi: 10.1016/S0025-3227(01)00114-1.

Mutti, E. (1992) Turbidite sandstones. Agip, Istituto di geologia, Università di Parma, Italy, 275 pp.

Normark, W.R. (1990) Return to Ranger Submarine Slide, Baja California, Mexico. *Geo-Marine Letters,* **10**, 81-91

Normark, W.R. and **Gutmacher, C.E.** (1988) Sur submarine slide, Monterey fan, central California. *Sedimentology,* **35**, 629-647.

Oelofsen, B.W. (1987) The biostratigraphy and fossils of the Whitehill and Irati Shale Formations of the Karoo and Paraná Basins. In: G*ondwana Six: Stratigraphy, Sedimentology and Palaeontology* (Ed. G. D., McKenzie), *Geophysical Monograph American Geophysical Union*, **41**, 131-138.

Ogiesoba, O. and **Hammes, U.** (2012) Seismic interpretation of mass-transport deposits within the upper Oligocene Frio Formation, south Texas Gulf Coast. *AAPG Bulletin*, **96**, 845-868.

Ortiz-Karpf, A., Hodgson, D.M. and **McCaffrey, W.D.** (2015) The role of mass-transport complexes in controlling channel avulsion and the subsequent sediment dispersal patterns on an active margin: the Magdalena Fan, offshore Colombia. *Marine and Petroleum Geology*, **64**, 58-75.

Ortiz-Karpf, A., Hodgson, D.M., Jackson, C.A.L. and **McCaffrey, W.D.** (2017a) Influence of seabed morphology and substrate composition on mass-transport flow processes and pathways: insights from the Magdelena fan, offshore Colombia. *Journal of Sedimentary Research*, **87**, 1-21.

Ortiz-Karpf, A., Hodgson, D.M., Jackson, C.A.L. and **McCaffrey, W.D.** (2017b) Mass-transport complexes as markers of deep-water fold-and-thrust belt evolution: insights from the southern Magdalena fan, offshore Colombia. *Basin Research.* DOI: 10.1111/bre.12208.

Pelinovsky, E. and **Poplavsky, A.** (1996) Simplified model of tsunami generation by submarine landslides. *Physics and Chemistry of the Earth*, **21**, 13-17.

Pickering, K.T. and **Corregidor, J.** (2005) Mass-transport complexes (MTCs) and tectonic control on basin-floor submarine fans, middle Eocene, south Spanish Pyrenees. *Journal of Sedimentary Research*, **75**, 761-783.

Pickering, K.T. and **Hiscott, R.N. (1985)** Contained (reflected) turbidity currents from the Middle Ordovician Cloridorme Formation, Quebec, Canada: an alternative to the antidune hypothesis. *Sedimentology,* **32**, 373-394.

Piper, D.J.W., Pirmez, C., Manley, P.L., Long, D., Flood, R.D., Normark, W.R. and **Showers, W.** (1997) Mass transport deposits of the Amazon Fan. I*n: Proceedings of the Ocean Drilling Program, Scientific Results* (Eds R.D. Flood, D.J.W. Piper, A. Klaus and L.C. Peterson) *Ocean Drilling Program, College Station, TX*, **155** 109–146.

Piper, D.J.W., Deptuck, M.E., Mosher, D.C., Hughes Clarke, J.E. and **Migeon, S**. (2012) Erosional and depositional features of glacial meltwater discharges on the eastern Canadian continental margin. In: *Applications of the Principles of Seismic Geomorphology to Continental Slope and Base-of-slope Systems: Case Studies from Seafloor and Near-Seafloor Analogues* (Eds B.E. Prather, M.E. Deptuck, D. Mohrig, B. van Hoorn, and R. Wynn) *Society for Sedimentary Geology (SEPM), Special Publications,* **99**, 61-80.

Posamentier, H.W. and **Kolla, V.** (2003) Seismic geomorphology and stratigraphy of depositional elements in deep-water settings. *Journal of Sedimentary Research*, **73**, 367-388.

Posamentier, H.W. and **Martinsen, O.J.** (2011) The character and genesis of submarine mass-transport deposits: insights from outcrop and 3D seismic data. In: *Mass-Transport Deposits in Deepwater Settings* (Eds R.G. Shipp, P. Weimer, H.W. Posamentier), *Society for Sedimentary Geology (SEPM) Special Publication,* **96**, 7-38.

Poyatos-Moré, M., Jones, G.D., Brunt, R.L., Hodgson, D.M., Wild, R.J. and **Flint, S.S.** (2016) Mud-dominated basin-margin progradation: processes and implications. *Journal of Sedimentary Research,* **86**, 863-878.

Prélat, A., Hodgson, D.M. and **Flint, S.S.** (2009) Evolution, architecture and hierarchy of distributary deep-water deposits: a high-resolution outcrop investigation from the Permian Karoo Basin, South Africa. *Sedimentology*, **56**, 2132-2154.

Prior, D.B., Bornhold, B.D. and **Johns, M.W.** (1984) Depositional characteristics of a submarine debris flow. *The Journal of Geology*, **92**, 707-727.

Qin, Y., Alves, T., Constantine, J.A. and **Gamboa, D.** (2017) The role of mass wasting in the progressive development of submarine channels (Espírito Santo Basin, SE Brazil). *Journal of Sedimentary Research*, **87**, 500-516, DOI: 10.2110/jsr.2017.18

Scheffler, K., Buehmann, D. and **Schwark, L.** (2006) Analysis of late Palaeozoic glacial to postglacial sedimentary successions in South Africa by geochemical proxies–response to climate evolution and sedimentary environment. *Palaeogeography, Palaeoclimatology, Palaeoecology,* **240**, 184-203.

Shipp, R.C., Nott, J.A. and **Newlin, J.A.** (2004) Physical characteristics and impact of mass transport complexes on deepwater jetted conductors and suction anchor piles. In: *OTC Paper 16751, p. 11 Annual Offshore Technology Conference, Houston, Texas.*

Shultz, M.R., Fildani, A., Cope, T.D. and **Graham, S.A.** (2005) Deposition and stratigraphic architecture of an outcropping ancient slope system: Tres Pasos Formation, Magallanes Basin, southern Chile. In: *Submarine Slope Systems: Processes and Products* (Eds. D.M. Hodgson and S.S. Flint), *Geological Society, London, Special Publications,* **244**, 27-50.

Sinclair, H.D. and **Cowie, P.A.** (2003) Basin-floor topography and the scaling of turbidites. *The Journal of Geology*, **111**, 277-299.

Sinclair, H.D. and **Tomasso, M.** (2002) Depositional evolution of confined turbidite basins. *Journal of Sedimentary Research*, **72**, 451-456.

Sixsmith, P.J., Flint, S.S., Wickens, H.D. and **Johnson, S.D.** (2004) Anatomy and stratigraphic development of a basin floor turbidite system in the Laingsburg Formation, main Karoo Basin, South Africa. *Journal of Sedimentary Research*, **74**, 239-254. doi: 10.1306/082903740239.

Smith, N.D. and **Ashley, G.** (1985) Proglacial lacustrine environment. In: *Glacial Sedimentary Environments* (Eds. G.M. Ashley, J. Shaw, and N.D. Smith), *SEPM Short Course*, **16**, 135–216.

Sobiesiak, M.S., Kneller, B., Alsop, G.I. and **Milana, J.P**. (2016) Internal deformation and kinematic indicators within a tripartite mass transport deposit, NW Argentina. *Sedimentary Geology*, **344**, 364-381.

Solheim, A., Berg, K., Forsberg, C.F. and **Bryn, P.** (2005) The Storegga Slide Complex: repetitive large scale sliding with similar cause and development. *Marine and Petroleum Geology*, **22**, 97-107. doi:10.1016/j.marpetgeo.2004.10.013

Southard, J.B. (1991) Experimental determination of bed-form stability*. Annual Review of Earth and Planetary Sciences,* **19**, 423-55

Spikings, A.L., Hodgson, D.M., Paton, D.A. and **Spychala, Y.T.** (2015) Palinspastic restoration of an exhumed deepwater system: A workflow to improve paleogeographic reconstructions. *Interpretation*, **3**, SAA71-SAA87.

Spörli, K.B. and **Rowland, J.V.** (2007) Superposed deformation in turbidites and syn-sedimentary slides of the tectonically active Miocene Waitemata Basin, northern New Zealand. *Basin Research*, **19**, 199-216.

Sprague, A.R., Sullivan, M.D., Campion, K.M., Jensen, G.N., Goulding, F.J., Garfield, T.R., Sickafoose, D.K., Rossen, C. and **Jennette, D.C.** (2002). The physical stratigraphy of deep-water strata: A hierarchical approach to the analysis of genetically-related stratigraphic elements for improved reservoir prediction. *National AAPG/SEPM meeting abstracts, Houston, Texas,* 10–13.

Spychala, Y.T., Hodgson, D.M., Flint, S.S. and **Mountney, N.P.** (2015) Constraining the sedimentology and stratigraphy of submarine intraslope lobe deposits using exhumed examples from the Karoo Basin, South Africa. *Sedimentary Geology,* **322**, 67-81.

Stevenson, C.J., Jackson, C.A-L., Hodgson, D.M., Hubbard, S.M. and **Eggenhuisen, J.** (2015) Sediment bypass in deep-water systems. *Journal of Sedimentary Research*, **85**, 1058-1081. doi: 10.2110/jsr.2015.63.

Stow, D.A. and **Johansson, M.** (2002) Deep-water massive sands: nature, origin and hydrocarbon implications. *Marine and Petroleum Geology*, **17**, 145-174. doi: 10.1016/S0264-8172(99)00051-3.

Strydom, H.C. (1950) The geology and chemistry of the Laingsburg phosphorites. *Annales of the University of Stellenbosch*, **26A**, 267–285.

Tankard, A.J., Jackson, M.P.A., Eriksson, K.A., Hobday, D.K., Hunter, D.R. and **Minter, W.E.L.** (1982) *Crustal Evolution of Southern Africa*. Springer-Verlag, New York. 523 pp.

Tankard, A., Welsink, H., Aukes, P., Newton, R. and **Stettler, E.** (2009) Tectonic evolution of the Cape and Karoo basins of South Africa. *Marine and Petroleum Geology*, **26**, 1379-1412.

Urgeles, R., Canals, M. and **Masson, D.G.** (2001) Flank stability and processes off the western Canary Islands: a review from El Hierro and La Palma. *Scientia Marina*, **65** (Supplement 1), 21-31.

van der Merwe, W.C., Hodgson, D.M. and **Flint, S.S.** (2009) Widespread syn-sedimentary deformation on a muddy deep-water basin-floor: the Vischkuil Formation (Permian), Karoo Basin, South Africa. *Basin Research*, **21,** 389-406. doi: 10.1111/j.1365-2117.2009.00396.x.

van der Merwe, W., Flint, S. and **Hodgson, D.** (2010) Sequence stratigraphy of an argillaceous, deepwater basin plain succession: Vischkuil Formation (Permian), Karoo Basin, South Africa. *Marine and Petroleum Geology*, **27**, 321-333. doi: 10.1016/j.marpetgeo.2009.10.007.

van der Merwe, W.C., Hodgson, D.M. and **Flint, S.S**. (2011) Origin and terminal architecture of a submarine slide: a case study from the Permian Vischkuil Formation, Karoo Basin, South Africa. *Sedimentology*, **58**, 2012-2038.

van der Merwe, W.C., Hodgson, D.M., Brunt, R.L. and **Flint, S.S.** (2014) Depositional architecture of sand-attached and sand-detached channel-lobe transition zones on an exhumed stepped slope mapped over a 2500 km^2 area. *Geosphere*, **10**, 1076-1093. doi: 10.1130/GES01035.1.

Vanneste, M., Mienert, J. and **Bünz, S.** (2006) The Hinlopen Slide: a giant, submarine slope failure on the northern Svalbard margin, Arctic Ocean. *Earth and Planetary Science Letters*, **245**, 373-388.

Varnes, D.J. (1958) Landslide types and processes. In: *Landslides and Engineering Practice* (Ed. E.B. Eckel). Highway research board special report, **29**, 20-47.

Varnes, D.J. (1978) Slope movement types and processes. In: *Landslides, Analysis and Control, Special Report 176* (Eds R.L. Schuster and R.J. Krizek), pp. 11-33. National Academy of Sciences, Washington.

Viljoen, J.H.A. (1992) Lithostratigraphy of the Collingham Formation (Ecca Group), including the Zoutkloof, Buffels river and Wilgenhout river members and the Matjiesfontein chert bed. *Geological Survey, South African Committee for Stratigraphy, Lithostratigraphic Series no. 22,* pp. 10.

Viljoen, J.H.A. (1994) Sedimentology of the Collingham Formation, Karoo Supergroup. *South African Journal of Geology*, **97**, 167-183.

Visser, J.N.J. (1979) Changes in sediment transport direction in the Cape Karoo Basin (Silurian-Triassic) in South Africa. *South African Journal of Science*, **75**, 72–75.

Visser, J.N.J. (1991) Self-destructive collapse of the Permo-Carboniferous marine ice sheet in the Karoo Basin: evidence from the southern Karoo. *South African Journal of Geology,* **94**, 255–262.

Visser, J.N.J. (1992) Basin tectonics in southwestern Gondwana during the Carboniferous and Permian. In: *Inversion tectonics of the Cape fold belt, Karoo and Cretaceous basins of southern Africa* (Eds M.J. de Wit and I.G.D. Ransome), pp 109-116. Balkema, Rotterdam.

Visser, J.N. (1993) Sea-level changes in a back-arc-foreland transition: the late Carboniferous-Permian Karoo Basin of South Africa. *Sedimentary Geology*, **83**, 115-131.

Visser, J.N.J. (1994) A Permian argillaceous syn- to post-glacial foreland sequence in the Karoo Basin, South Africa. In: *Earth's Glacial Record, International Geological Correlation Project* (Eds M. Deynoux, J.M.G, Miller, E.W. Domack, N. Eyles, I.J. Fairchild, G.M. Young), **260,** 193- 203. Cambridge University Press, Cambridge.

Visser, J.N.J. (1997) Deglaciation sequences in the Permo-Carboniferous Karoo and Kalahari basins of the southern Africa: a tool in the analysis of cyclic glaciomarine basin fills. *Sedimentology*, **44**, 507–521. doi: 10.1046/j.1365-3091.1997.d01-35.x.

Visser, J.N.J. and **Prackelt, H.E.** (1996) Subduction, mega-shear systems and Late Palaeozoic basin development in the African segment of Gondwana. *Geologische Rundschau*, **85**, 632–646. doi: 10.1007/BF02440101.

Woodcock, N.H. (1979) The use of slump structures as palaeoslope orientation estimators. *Sedimentology*, **26**, 83-99.

Figure Captions

Figure 1- Example of a submarine landslide including a basal shear surface or zone with confining lateral margins from a 3D seismic volume of upper to mid slope deposits, Magdalena Fan, Caribbean Sea, offshore Colombia. (A) Variance extraction map of submarine landslide. (B) Seismic cross sections through submarine landslide highlighting the erosional basal shear surface/zone and depositional relief at the top of the initial remobilized/ mass transport deposits or mass transport complex (MTC) fill and overlying/onlapping turbidites. The basal shear surface or zone widens and shallows down-dip with lateral margins showing a decrease in gradient (adapted from Ortiz-Karpf et al., 2017a).

Figure 2- (A) Image of southwestern Karoo Basin showing Tanqua and Laingsburg depocentres outlined and study area enlarged. (B) Enlargement of outcrop section showing data points and outcrop location. Sections east and west of the zones of no exposure/ tectonic deformation show in place strata unaffected by large-scale erosion surfaces. (C) (Left) Stratigraphic column of Late Carboniferous, Permian and Early Triassic deposits in the Laingsburg depocentre. Blue dashed box indicates units involved in this study. (Right) Logged section of strata outside of outcrop, showing in place deposit, unaffected by large-scale erosion. Lower logged units correspond to the Whitehill, Collingham and Vischkuil formations. Upper units of thick remobilized sandstone and bedded turbidites may correspond to the Vischkuil/ Laingsburg Formations or the equivalent formations to the East.

Figure 3- (A) Logs and correlation of units across outcrop. Colours indicate facies associations, red lines show observed and interpreted surfaces. Numbers indicate package divisions. Log of Surface 2 infill (Packages 4 and 5) shown in figure 9. (B) Photopanel of outcrop with overlay of logged sections, facies associations and erosional surfaces.

Figure 4- Representative photographs depicting facies associations present throughout the outcrop. (A) Iron-rich mudstone, Prince Albert Formation. (B) Organic rich mudstone, Whitehill Formation, notebook shown 20 cm long. (C) Iron cemented sandstone turbidite beds. (D) Matjiesfontein chert, marker bed, lens cap 7 cm in diameter. (E) Interbedded sandstone/ siltstone turbidites and ash deposits (marked as A), notebook 20 cm long. (F) Interbedded turbidites and chert layers, notebook 20 cm long. (G) Sharp topped sandstone and siltstone beds, upper turbidite marker package. (H) Sandstone to siltstone graded turbidite beds. (I) Thin-bedded turbidites. (J) Planar and climbing ripple laminated turbidite. (K) Iron-rich ripple laminated turbidite. (L) Thick debrite. (M) Section of

debrite with mm- cm scale mudstone clast in distinctive blue mud-rich matrix, pencil for scale. (N) Folded interbedded sandstone and siltstone turbidites, geologist for scale. (O) Folded and slumped sandstone beds, white dashed lines indicates fold of beds, geologist for scale. (P) Base of folded sandstone bed.

Figure 5- Sketches illustrating stratigraphic evolution, divided into 7 key stages. (P1) Deposition of lower Ecca group, folded and chaotic strata and megaclasts. (S1) Formation of surface 1, (P2) overlain by folded, chaotic deposits and clasts. (P3) Deposition of onlapping and infilling turbidites and chaotic strata. (S2) Formation of surface 2. (P4) Infill of surface by chaotic deposits. (P5) Deposition of onlapping and infilling turbidites and folded strata.

Figure 6- Photo of lower stratigraphy, Collingham Fm. with Matjiesfontein chert bed, decreasing upwards in ash and chert with a transitional boundary to overlying silt-rich turbidites. A sharp, slightly erosive boundary marks the deposition of chaotic and remobilized strata.

Figure 7- Key architectural characteristics across outcrop. (A) Lower stratigraphy (Package 1) cut by Surface 1, which passes from a sharp, stepped surface to intense zone of sheared mudrock laterally (detailed photo shown in figure 8A), overlain by onlapping turbidites and chaotic deposits (Package 3), cut by Surface 2, overlain by chaotic deposits and megaclast (Package 4) and further overlain by onlapping graded turbidites, chaotic packages and upper turbidite package datum (Package 5). (B) Collingham clast (Package 2) overlain by onlapping but rotated turbidites (Package 3), cut by Surface 2 and overlain by debrites and further onlapping turbidites (Package 4). (C) Debrite and slumps (Package 2) overlain by megaclasts (Package 2) and debrites(Package 3), cut by Surface 2 overlain by debrites (Package 4) and onlapping, graded turbidites (Package 5). Facies association colour key shown on figure 3.

Figure 8- Photos basal shear zone (Surface 1) and slumped sandstone-rich turbidites and surface 2. (A) Section of basal shear zone with foiled fabric, contorted strata, sheath folds and white lines showing numerous small scale faults. (B) Stepped section of surface 2 cutting folded and dewatered sandstone turbidites (Package 3). Overlying turbidites onlap surface (Package 5). (C) Erosional surface eroding slumped sandstone (Package 3) overlain by Collingham clast (Package 4). (D) Stepped surface 2 with onlapping turbidites (Package 5) from opposing sides of topography. (E) Scour present on top of erosional surface with coarse lag of medium sandstone and mudclasts. (F) Scour on top of erosional surface mantled with mudstone clasts.

Figure 9- Logged section through Package 4 and Package 5. Base of log is Surface 2. Location of log shown on figure 3 and 7C. Chaotic deposits of Package 4 are overlain by thick graded turbidite beds

which transition upwards into thinner sharp topped beds with intervening layers of chaotic and folded deposits that are laterally extensive over the outcrop. Top 12 m of log are used as upper datum for figure 3. Key for facies association on figure 3.

Figure 10- Sketches illustrating depositional and erosional evolution over the outcrop and the surrounding area, with sequential panels simplified from figure 3. (P1i) Deposition of lower Ecca Group stratigraphy towards the east. (P1ii) Unconfined remobilized deposition. (S1 & P2) Erosion and deformation by Surface 1 and remobilized infill towards the north. (P3i) partially confined turbidite infill, with overlying chaotic deposits. (P3ii) Partially remobilized intraslope lobe complex. (S2 & P4) Erosion and deformation by Surface 2 and chaotic infill. (P4i) Fully confined turbidite and chaotic infill of surface 2. (P5ii) Overspill of confining topography and unconfined turbidite deposition.

Figure 11- Post deposition failure of basal shear surfaces/ zones. Including tilting of onlapping strata and failure away from lateral margins and headwall. Both Surface 1 and 2 basal shear varies from a distinct surface to zone of intense shaear when eroding into coarser sediment (sharp/ stepped) or finer material (chaotic zone of shear). Dashed brackets numbered 1-3 refer to slide complex subdivisions (Stage 1, 2 and 3), discussed in text and shown in figure 12.

Figure 12- Three key stages of outcrop evolution. Stage 1- deposition of frontally emergent remobilized deposits with onlapping turbidity currents, with basal shear surface/zone located up-dip of the outcrop exposure in this study. Stage 2- Formation of basal shear surface/zone 1, with initial remobilized deposits either frontally confined with frontal ramp creating down-dip topography or frontally emergent and creating a mounded topographic barrier down-dip. Subsequent infilling turbidites are partially confined. Stage 3- Formation of basal shear surface/zone 2 with initial remobilized deposits either frontally confined with frontal ramp creating down-dip topography or frontally emergent and creating a mounded topographic barrier down-dip. Subsequent turbidite and remobilized infill transitions stratigraphically from fully confined to unconfined.

Figure 13- (A) Simplified dip section of Stage 1, 2 and 3 basal shear surfaces/zones and subsequent deposits, showing possible scenario to create strike section documented in this study. (B) Evolution of turbidite confinement from Stages 1-3 showing transition from unconfined turbidites, to partially confined and fully confined with each subsequent failure. Dip section shows how increasing slope gradient and mounding of deposits down-dip could create increased turbidite confinement whilst initial remobilized deposits remain frontally emergent with decreasing run-out distance.

Figure 14- Sketch of shelf and slope systems indicating how interplay of sediment supply rate and rate of slope degradation can vary the infill of submarine landslides. Slides in areas of high sediment supply can cause the capture and rerouting of sediment pathways, and become quickly infilled and overspilled. In locations distal to sediment supply, slides can remain underfilled with degradation rate outpacing sedimentation rate. In intermediary areas periods of high and low sediment supply mean that on average sediment supply is roughly equal to degradation rate.

Figure 1

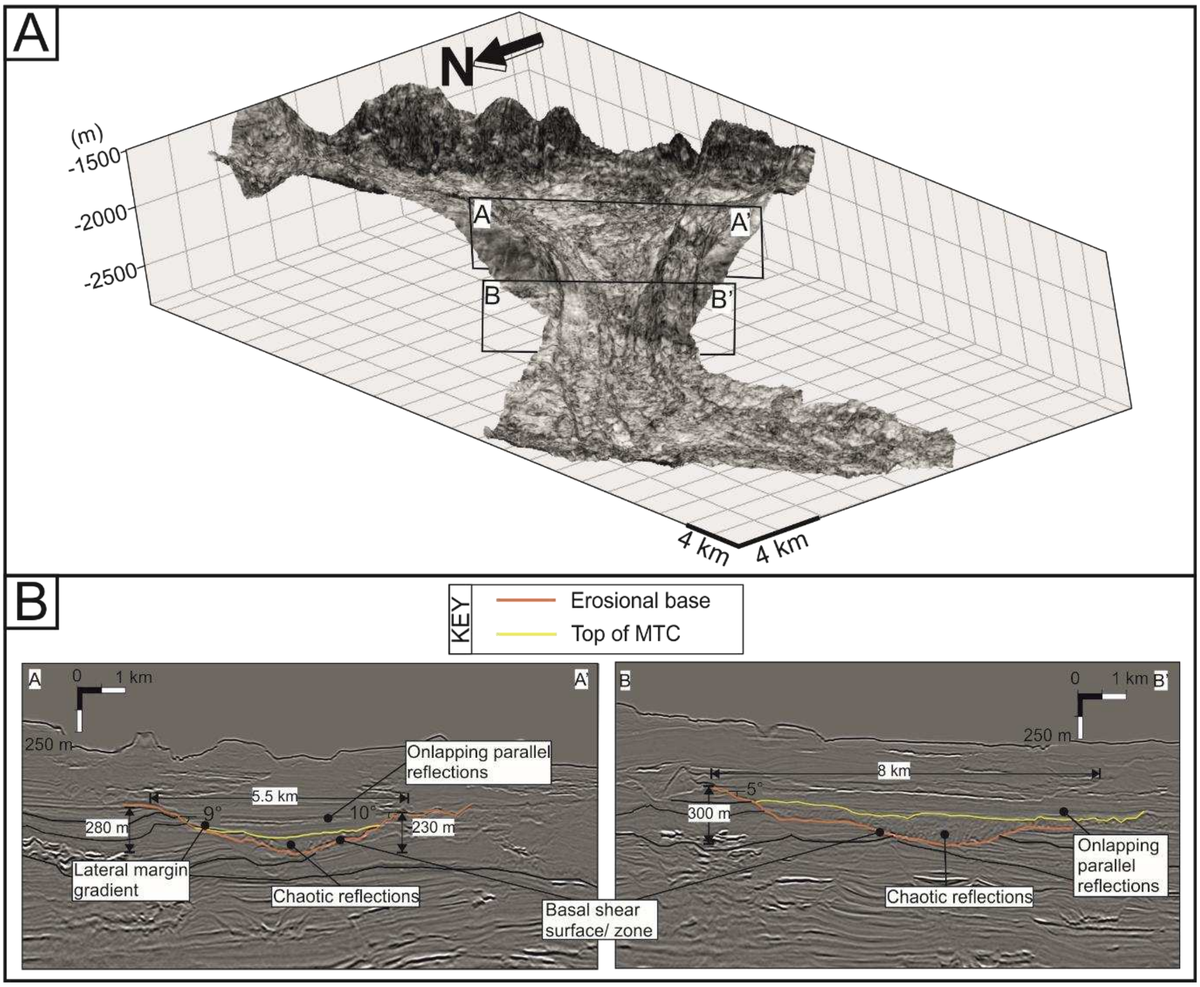

1196 Figure 2

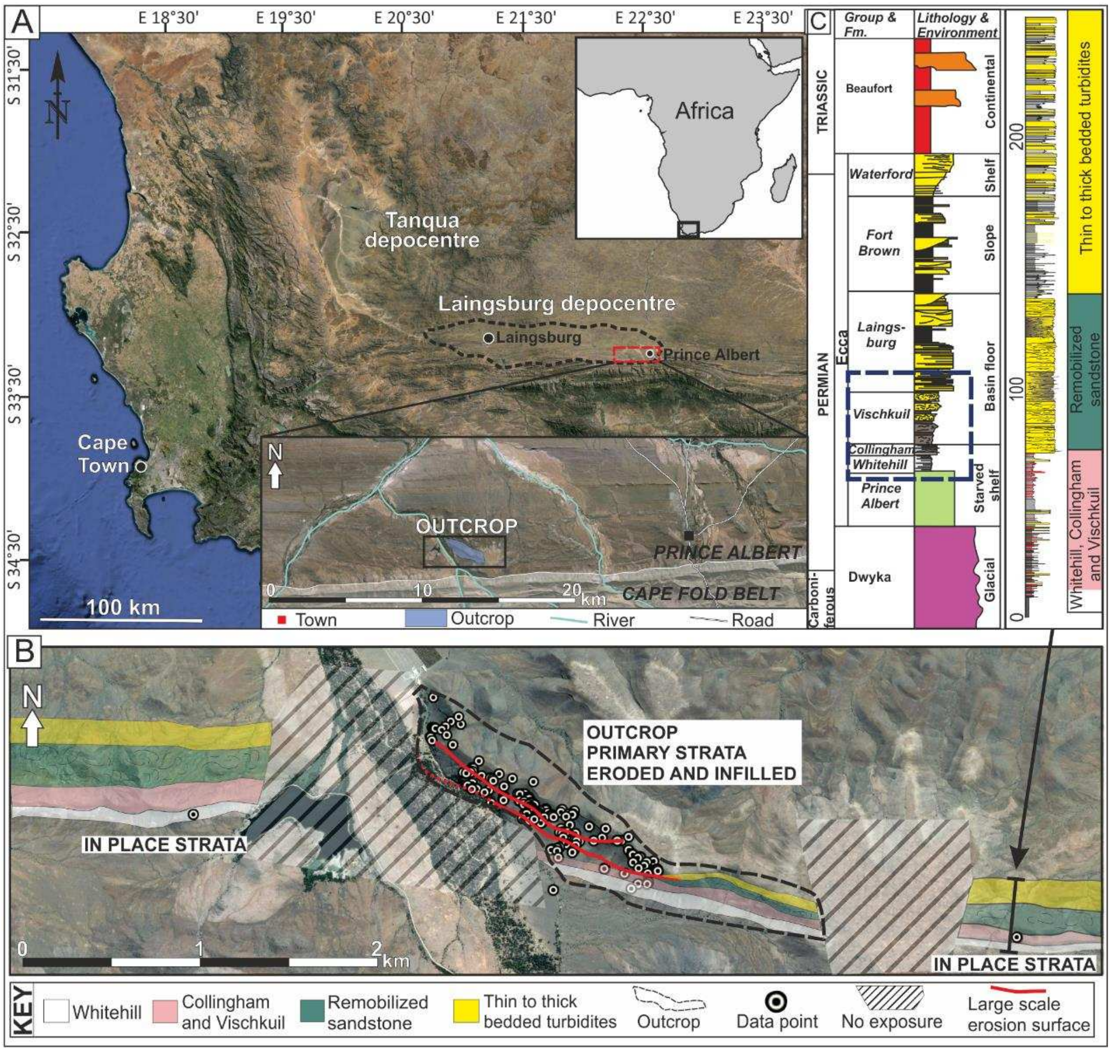

1197

1198

Figure 3

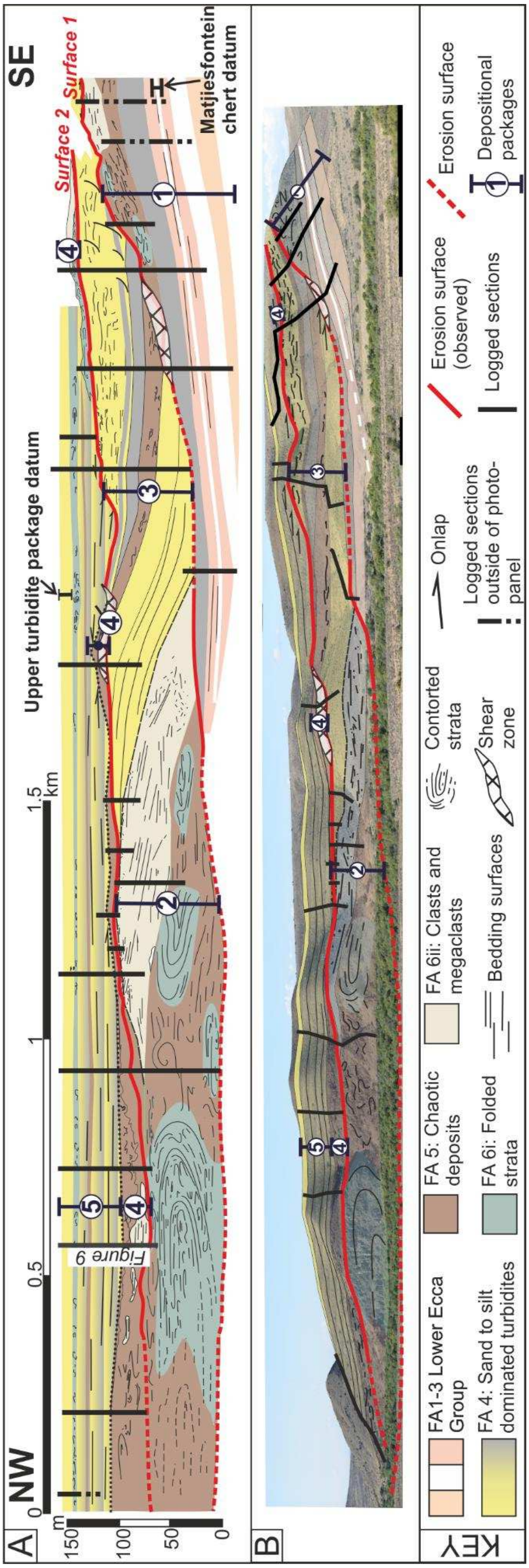
A
B
KEY
NW
SE
m
150
100
50
0
0
0.5
1
1.5
km
Surface 1
Surface 2
Matjiesfontein chert datum
Upper turbidite package datum
Figure 9
1
2
3
4
5
FA1-3 Lower Ecca Group
FA 4: Sand to silt dominated turbidites
FA 5: Chaotic deposits
FA 6i: Folded strata
FA 6ii: Clasts and megaclasts
Bedding surfaces
Contorted strata
Shear zone
Onlap
Logged sections outside of photo-panel
Erosion surface (observed)
Logged sections
Erosion surface
Depositional packages

Figure 4

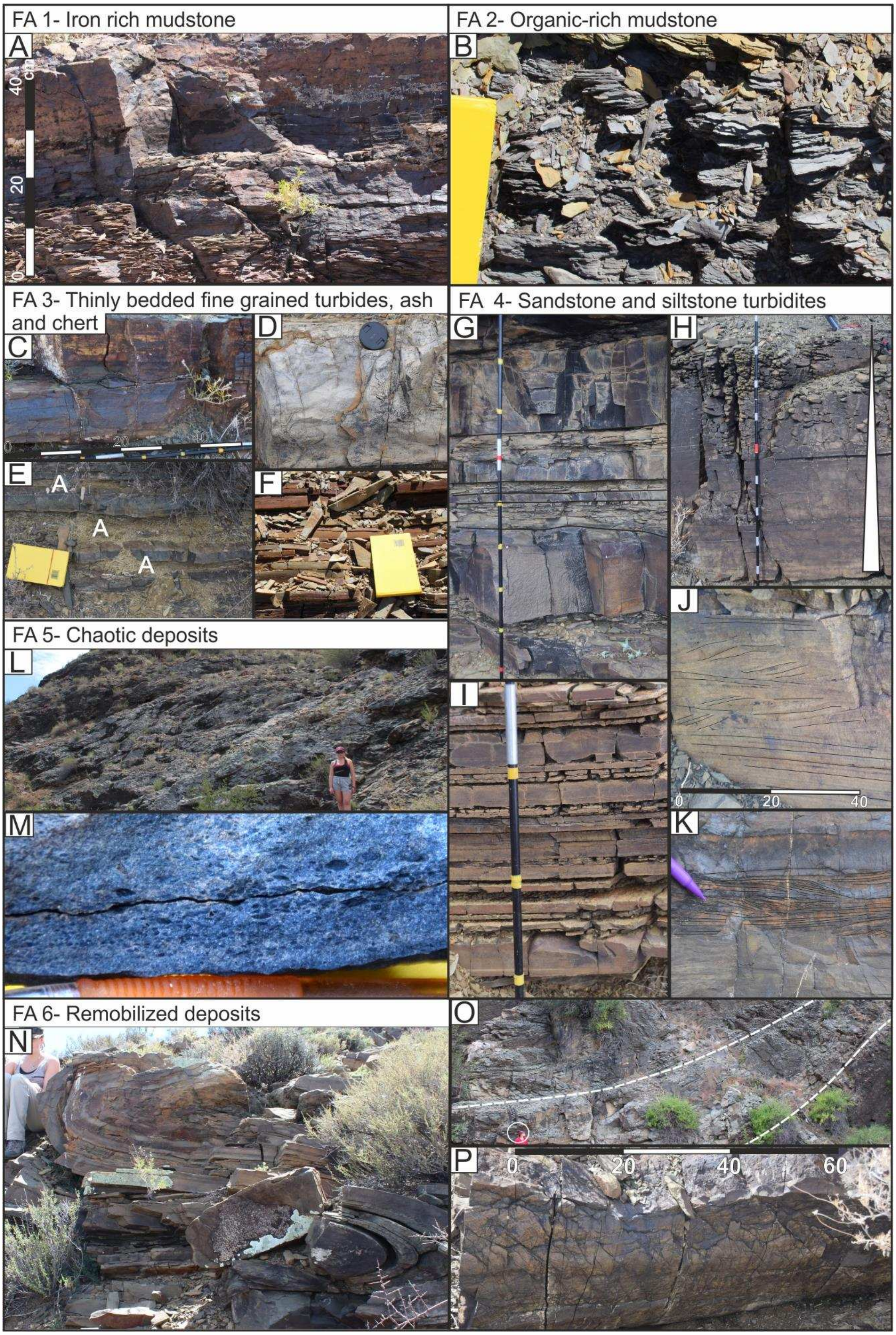

FA 1- Iron rich mudstone
A
40 cm
20
0
FA 2- Organic-rich mudstone
B
FA 3- Thinly bedded fine grained turbides, ash and chert
C
0
20
40
D
E
A
A
A
F
FA 4- Sandstone and siltstone turbidites
G
H
I
J
0
20
40
K
FA 5- Chaotic deposits
L
M
FA 6- Remobilized deposits
N
O
P
0
20
40
60

1203 Figure 5

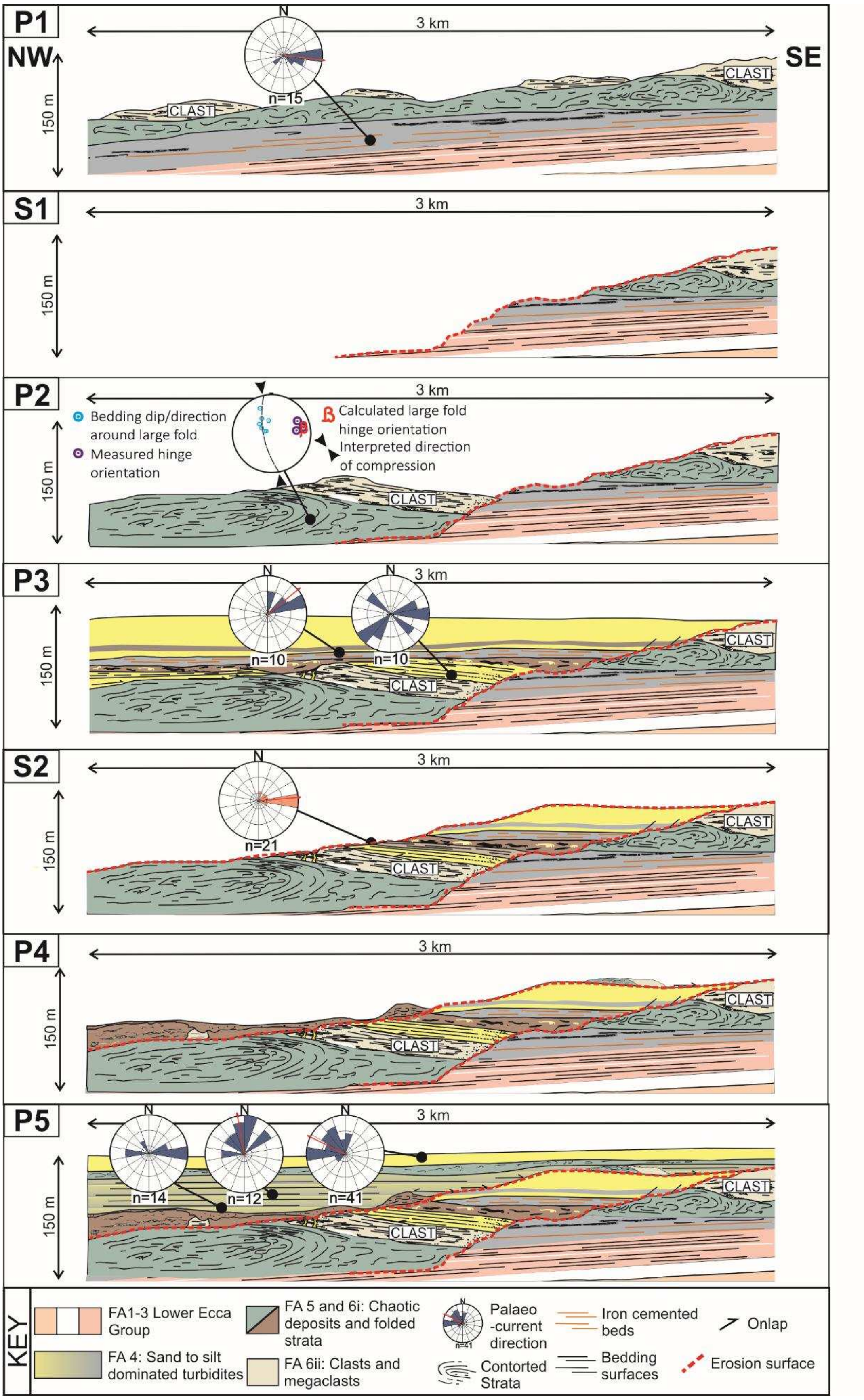

1204

1205

1206 Figure 6

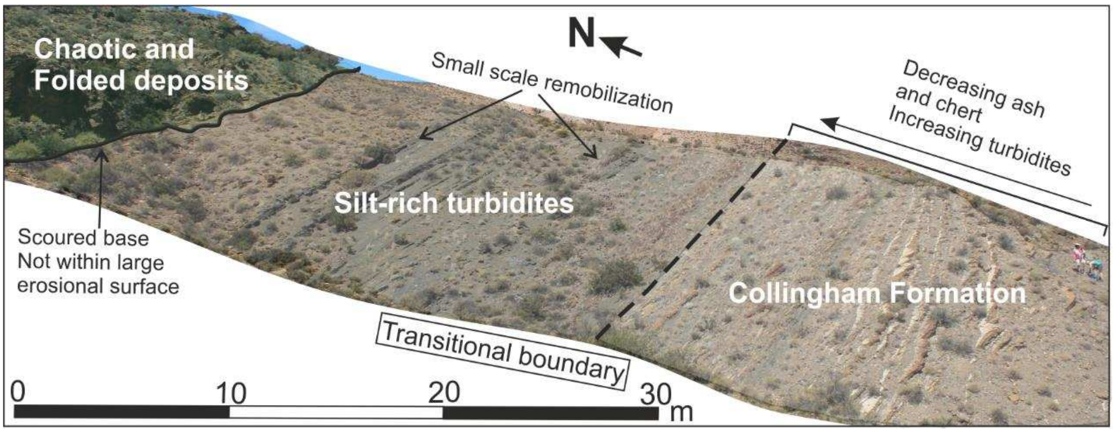

1207

1208 Figure 7

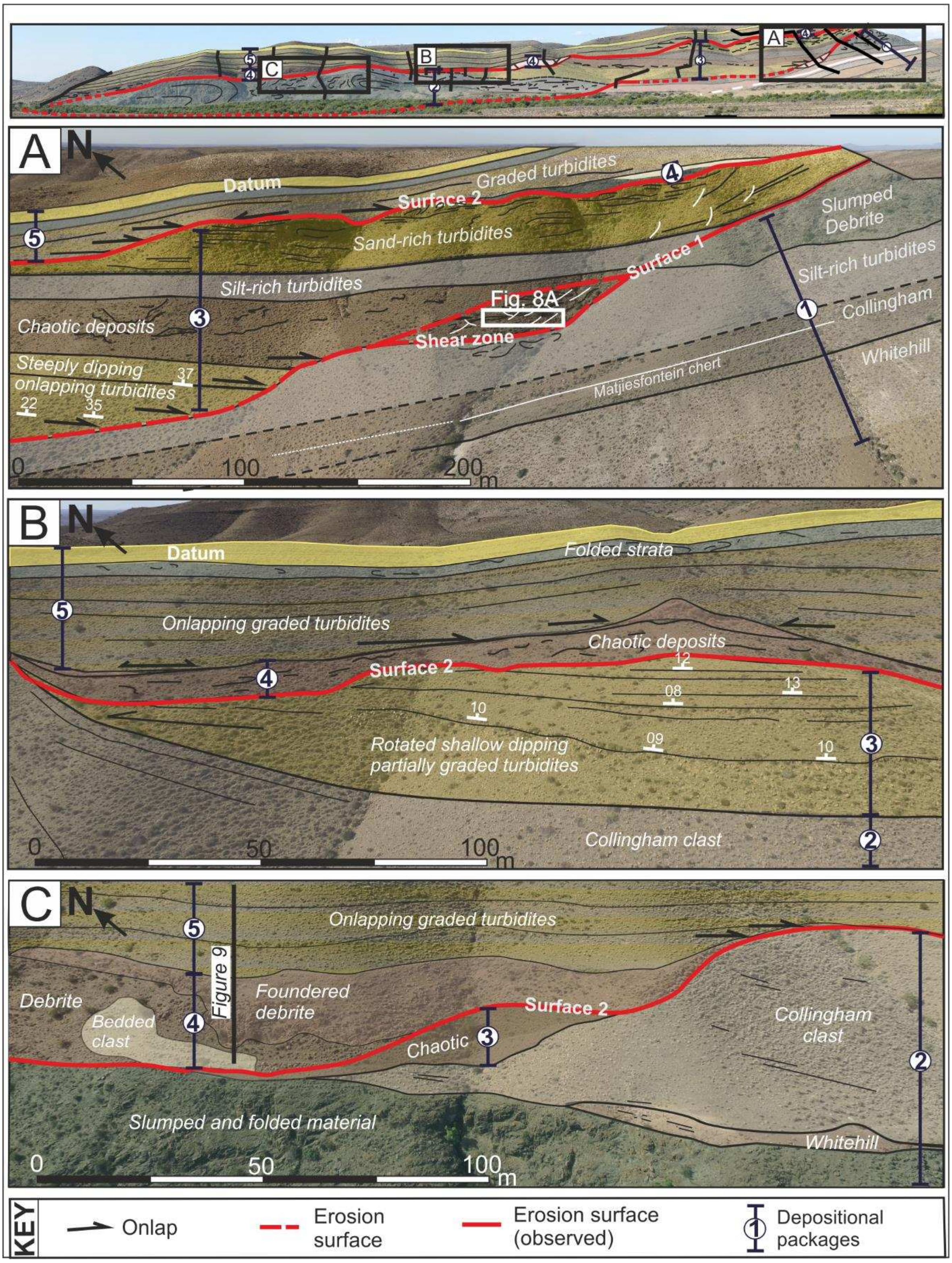

1209

1210 Figure 8

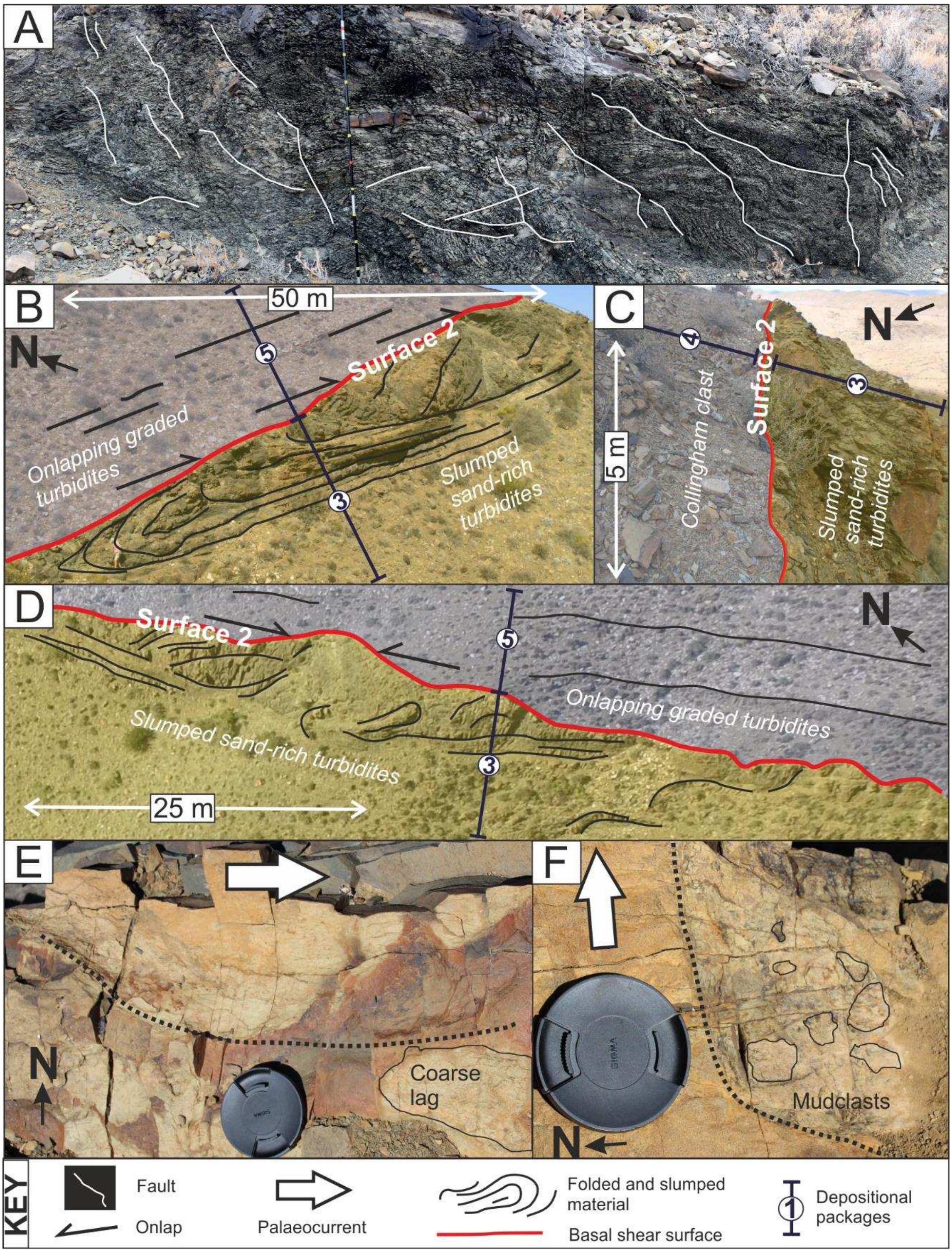

1211

1212 Figure 9

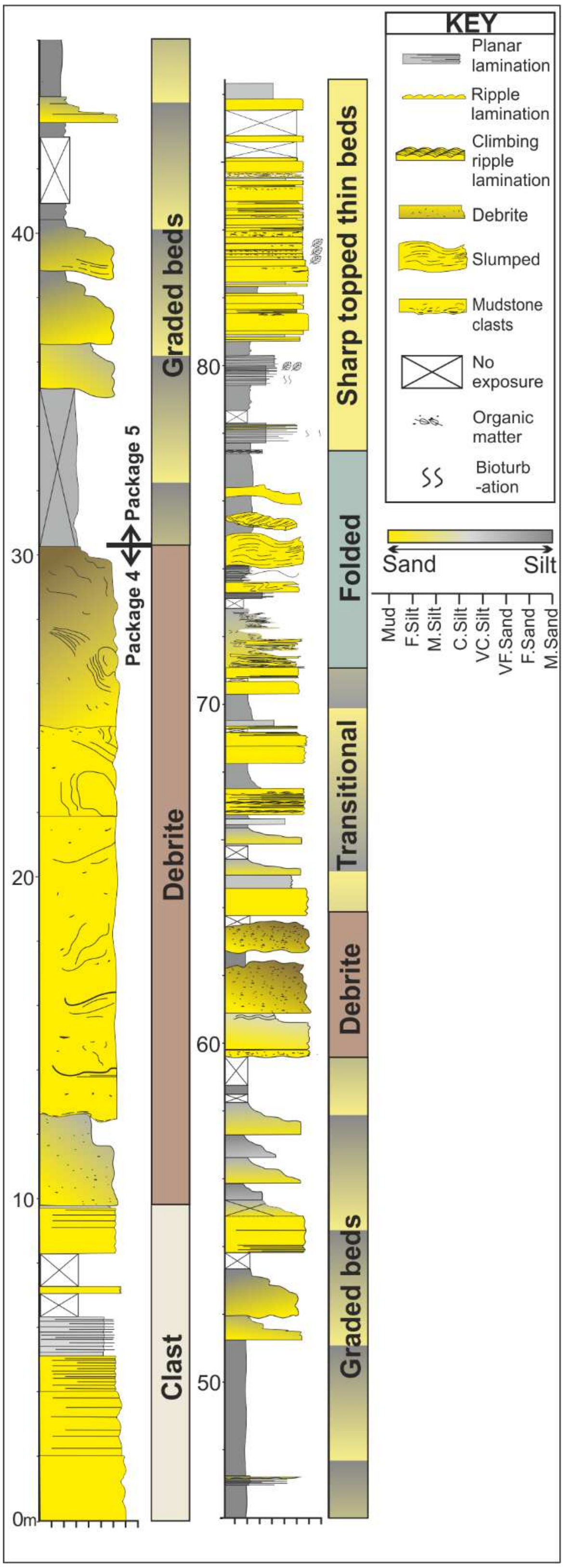

Figure 10

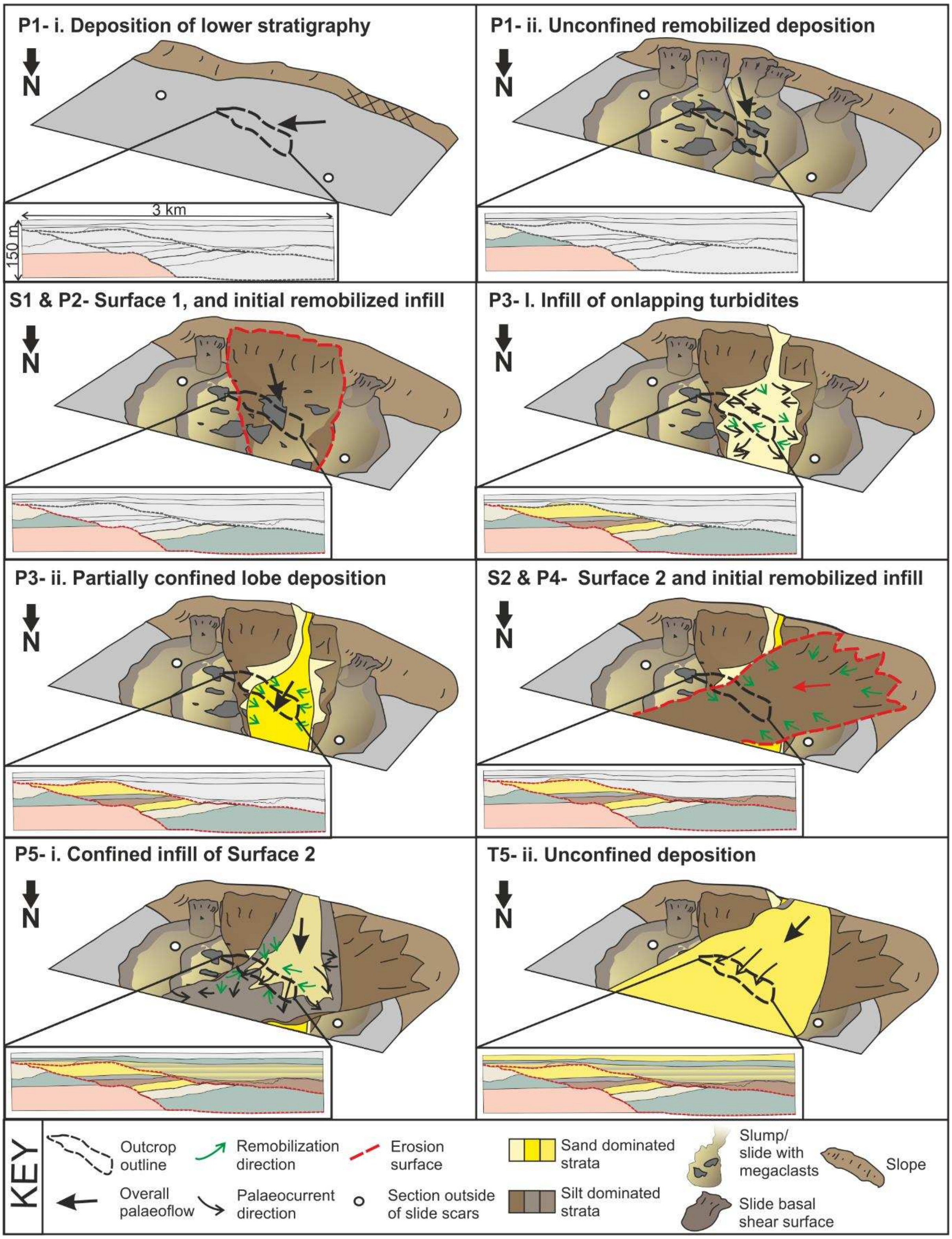

P1- i. Deposition of lower stratigraphy
N
3 km
150 m
P1- ii. Unconfined remobilized deposition
N
S1 & P2- Surface 1, and initial remobilized infill
N
P3- I. Infill of onlapping turbidites
N
P3- ii. Partially confined lobe deposition
N
S2 & P4- Surface 2 and initial remobilized infill
N
P5- i. Confined infill of Surface 2
N
T5- ii. Unconfined deposition
N
KEY
Outcrop outline
Overall palaeoflow
Remobilization direction
Palaeocurrent direction
Erosion surface
Section outside of slide scars
Sand dominated strata
Silt dominated strata
Slump/ slide with megaclasts
Slide basal shear surface
Slope

Figure 11

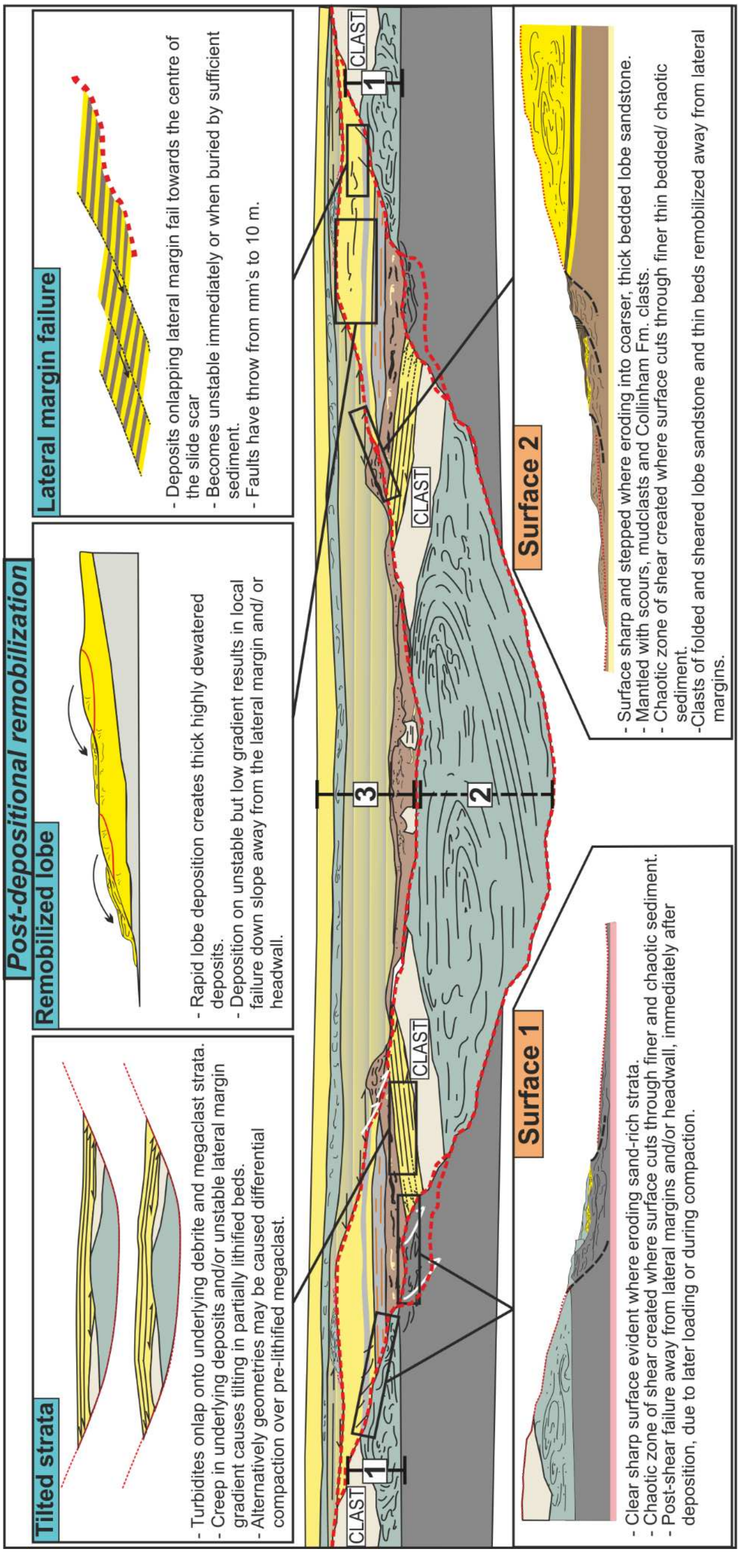
Post-depositional remobilization
Tilted strata
- Turbidites onlap onto underlying debrite and megaclast strata.
- Creep in underlying deposits and/or unstable lateral margin gradient causes tilting in partially lithified beds.
- Alternatively geometries may be caused differential compaction over pre-lithified megaclast.
Remobilized lobe
- Rapid lobe deposition creates thick highly dewatered deposits.
- Deposition on unstable but low gradient results in local failure down slope away from the lateral margin and/ or headwall.
Lateral margin failure
- Deposits onlapping lateral margin fail towards the centre of the slide scar
- Becomes unstable immediately or when buried by sufficient sediment.
- Faults have throw from mm's to 10 m.
CLAST
CLAST
CLAST
CLAST
1
1
2
3
Surface 1
- Clear sharp surface evident where eroding sand-rich strata.
- Chaotic zone of shear created where surface cuts through finer and chaotic sediment.
- Post-shear failure away from lateral margins and/or headwall, immediately after deposition, due to later loading or during compaction.
Surface 2
- Surface sharp and stepped where eroding into coarser, thick bedded lobe sandstone.
- Mantled with scours, mudclasts and Collinham Fm. clasts.
- Chaotic zone of shear created where surface cuts through finer thin bedded/ chaotic sediment.
-Clasts of folded and sheared lobe sandstone and thin beds remobilized away from lateral margins.

Figure 12

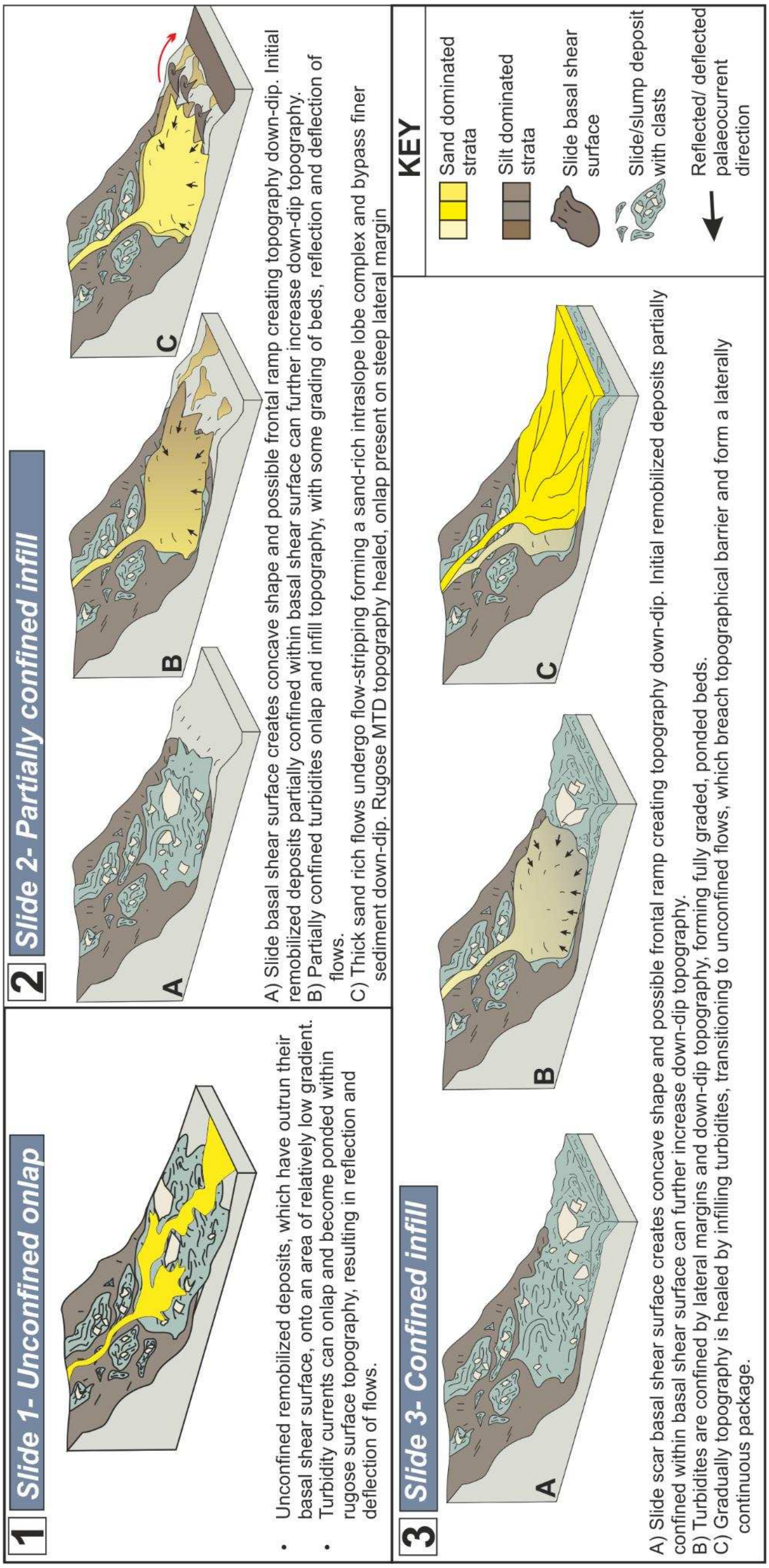
1 Slide 1- Unconfined onlap
Unconfined remobilized deposits, which have outrun their basal shear surface, onto an area of relatively low gradient.
Turbidity currents can onlap and become ponded within rugose surface topography, resulting in reflection and deflection of flows.
2 Slide 2- Partially confined infill
A
B
C
A) Slide basal shear surface creates concave shape and possible frontal ramp creating topography down-dip. Initial remobilized deposits partially confined within basal shear surface can further increase down-dip topography.
B) Partially confined turbidites onlap and infill topography, with some grading of beds, reflection and deflection of flows.
C) Thick sand rich flows undergo flow-stripping forming a sand-rich intraslope lobe complex and bypass finer sediment down-dip. Rugose MTD topography healed, onlap present on steep lateral margin
3 Slide 3- Confined infill
A
B
C
A) Slide scar basal shear surface creates concave shape and possible frontal ramp creating topography down-dip. Initial remobilized deposits partially confined within basal shear surface can further increase down-dip topography.
B) Turbidites are confined by lateral margins and down-dip topography, forming fully graded, ponded beds.
C) Gradually topography is healed by infilling turbidites, transitioning to unconfined flows, which breach topographical barrier and form a laterally continuous package.
KEY
Sand dominated strata
Silt dominated strata
Slide basal shear surface
Slide/slump deposit with clasts
Reflected/ deflected palaeocurrent direction

Figure 13

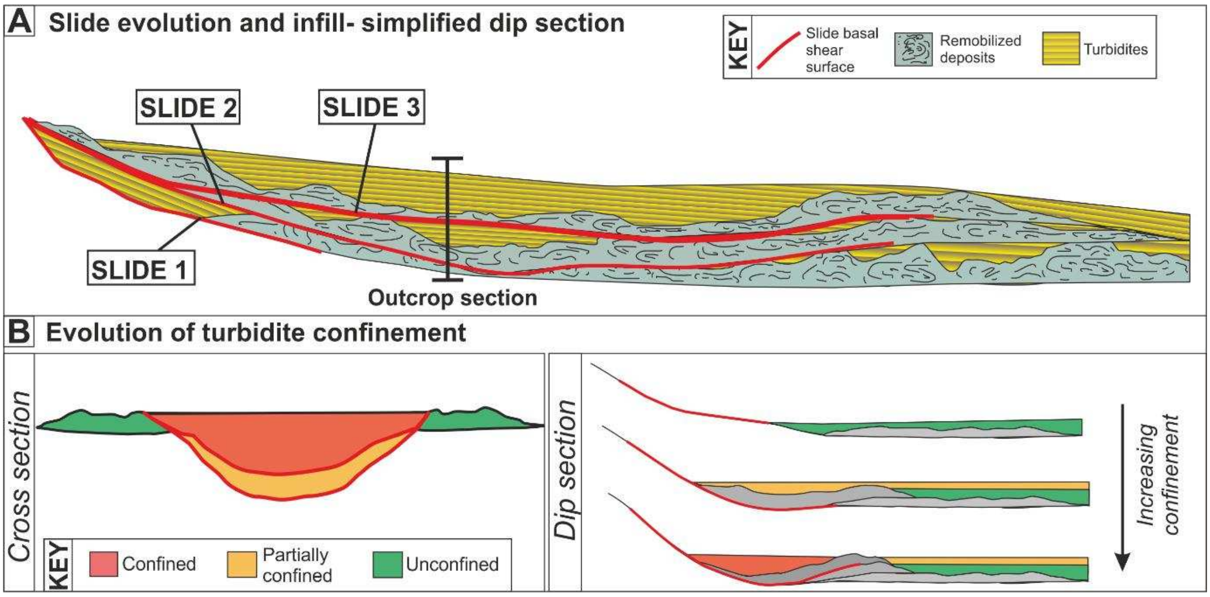

Figure 14